5-HT6 receptor neutral antagonists protect astrocytes: A lesson from 2-phenylpyrrole derivatives

Marcin Drop, Paulina Koczurkiewicz-Adamczyk, Ophélie Bento, Wojciech Pietruś, Grzegorz Satala, Klaudia Blicharz-Futera, Vittorio Canale, Katarzyna Grychowska, Xavier Bantreil, Elżbieta Pękala, et al.

European Journal of Medicinal Chemistry 275 (2024) 116615

Contents lists available at ScienceDirect

European Journal of Medicinal Chemistry

journal homepage: www.elsevier.com/locate/ejmech

Research paper

5-HT$_6$ receptor neutral antagonists protect astrocytes: A lesson from 2-phenylpyrrole derivatives

Marcin Drop [a,b], Paulina Koczurkiewicz-Adamczyk [a], Ophélie Bento [b,c], Wojciech Pietruś [d], Grzegorz Satała [d], Klaudia Blicharz-Futera [a], Vittorio Canale [a], Katarzyna Grychowska [a], Xavier Bantreil [b,e], Elżbieta Pękala [a], Rafał Kurczab [d], Andrzej J. Bojarski [d], Severine Chaumont-Dubel [c], Philippe Marin [c], Frédéric Lamaty [b], Paweł Zajdel [a,*]

[a] Faculty of Pharmacy, Jagiellonian University Medical College, 9 Medyczna Str., 30-688, Kraków, Poland
[b] IBMM, Université de Montpellier, CNRS, ENSCM, 34095, Montpellier, France
[c] Institut de Génomique Fonctionelle, Université de Montpellier, CNRS INSERM, 34094, Montpellier, France
[d] Maj Institute of Pharmacology, Polish Academy of Sciences, 12 Smętna Str., 31-343, Kraków, Poland
[e] Institut Universitaire de France (IUF), France

ARTICLE INFO

Keywords:
5-HT$_6$ receptor
Constitutive activity
Neutral antagonism
Inverse agonism
2-phenylpyrrole
Cytoprotection
Human astrocytes

ABSTRACT

The serotonin type 6 receptor (5-HT$_6$R) displays a strong constitutive activity, suggesting it participates largely in the physiological and pathological processes controlled by the receptor. The active states of 5-HT$_6$R engage particular signal transduction pathways that lead to different biological responses. In this study, we present the development of 5-HT$_6$R neutral antagonists at Gs signaling built upon the 2-phenylpyrrole scaffold. Using molecular dynamics simulations, we outline the relationship between the exposure of the basic center of the molecules and their ability to target the agonist-activated state of the receptor. Our study identifies compound **30** as a potent and selective neutral antagonist at 5-HT$_6$R-operated Gs signaling. Furthermore, we demonstrate the cytoprotective effects of **30** and structurally diverse 5-HT$_6$R neutral antagonists at Gs signaling in C8-D1A cells and human astrocytes exposed to rotenone. This effect is not observed for 5-HT$_6$R agonists or inverse agonists. In light of these findings, we propose compound **30** as a valuable molecular probe to study the biological effects associated with the agonist-activated state of 5-HT$_6$R and provide insight into the glioprotective properties of 5-HT$_6$R neutral antagonists at Gs signaling.

1. Introduction

The serotonergic system plays a crucial role in virtually all cerebral functions, and its dysregulation is implicated in the pathogenesis of numerous psychiatric and neurological disorders [1,2]. Among the seven major classes of serotonin receptors [3], the serotonin type 6 receptor (5-HT$_6$R) has garnered particular attention as a target for the development of new cognitive-enhancing agents [4]. The pro-cognitive effects of 5-HT$_6$R antagonists, attributed to their capacity to facilitate the corticolimbic release of acetylcholine, glutamate, and monoamines, have been demonstrated in a wide range of cognitive impairment paradigms in rodents [5,6]. Furthermore, 5-HT$_6$R antagonists have advanced to the later stages of clinical development for the treatment of mild to moderate Alzheimer's disease [7,8].

5-HT$_6$R belongs to the family of G-protein coupled receptors (GPCRs) and, beyond its canonical coupling to the Gs adenylyl cyclase pathway, it interacts with several protein partners to modulate a range of signal transduction pathways [9]. For instance, 5-HT$_6$R interacts with Fyn tyrosine kinase, which inhibits receptor internalization and enhances receptor-operated Gs and Erk1,2 signaling pathways [10]. Furthermore, 5-HT$_6$R recruits the mechanistic target of rapamycin (mTOR) complex, which regulates neuronal development, synaptic plasticity, memory storage, and cognition [11]. In rodent models of schizophrenia, this complex is overactivated in the prefrontal cortex and 5-HT$_6$R antagonists can reverse both the overactivation of the pathway and the phenotypes associated with it.

In addition to its broad interactome, 5-HT$_6$R shows a significant level of ligand-independent constitutive activity [12]. This ability of 5-HT$_6$R

* Corresponding author.Department of Organic Chemistry Jagiellonian University Medical College, Poland.
E-mail address: pawel.zajdel@uj.edu.pl (P. Zajdel).

https://doi.org/10.1016/j.ejmech.2024.116615
Received 26 April 2024; Received in revised form 20 June 2024; Accepted 20 June 2024
Available online 21 June 2024

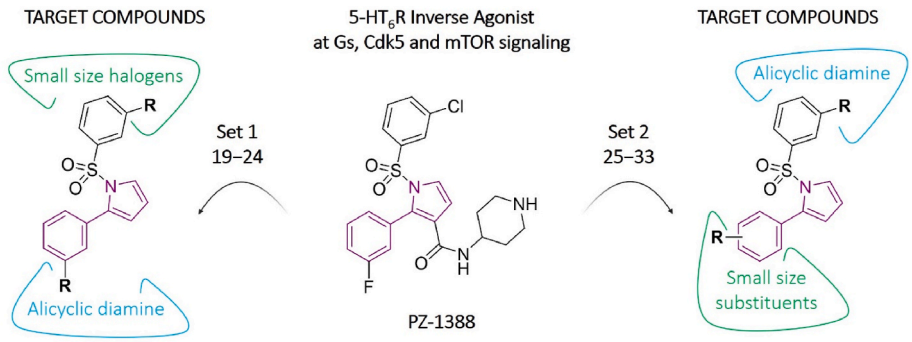

Fig. 1. Structural rearrangement around 2-phenyl-1*H*-pyrrole-3-carboxamide derivatives [24,25], with lead compound **PZ-1388** [26], providing the target compounds.

to display spontaneous activity in the absence of an agonist was initially demonstrated in vitro in recombinant receptors [13]. Subsequent validation of this phenomenon has been achieved in primary cultured neurons expressing native receptors and, notably, within the murine brain [14]. The constitutive activity of 5-HT$_6$R has been intricately linked to pivotal aspects of neuronal development [15], neocortical migration [16], and has demonstrated influence over the self-renewal processes of human neural stem cells [14]. Notably, 5-HT$_6$R interacts with and is phosphorylated by the cyclin-dependent kinase 5 (Cdk5), a serine/threonine kinase critical for neuron migration, microtubule regulation, cell cycle suppression, and memory formation [17]. The interaction is involved in neuronal differentiation and the initiation of neurite outgrowth induced by the receptor. This mechanism is completely constitutive: it doesn't require serotonin to be present, but is inhibited by inverse agonists of the receptor [13].

It was demonstrated that compounds that behave as 5-HT$_6$R partial agonists (EMD-386088) and 5-HT$_6$R antagonists (SB-399885) produce protective effects against Aβ_{25-35}-induced toxicity in PC-12 cells by reducing reactive oxygen species (ROS) [18]. Recently developed 1,3,5-triazine-based 5-HT$_6$R antagonists have shown protective effects against rotenone-induced neurotoxicity, as well as antioxidant and glutathione peroxidase (GPx)-like activity. They also regulate antioxidant and pro-inflammatory genes and NRF2 nuclear translocation [19]. Although these studies suggests the cytoprotective properties of 5-HT$_6$R ligands, the exact mechanisms associated with the effect remain unclear.

The existence of multiple conformations of 5-HT$_6$R has prompted us to establish the link between the active state of the receptor and protective effects for neurons and astrocytes. Our initial investigations in this field indicated a protective effect of selective 5-HT$_6$R neutral antagonists (based on imidazopyridine [20] and isoindoline [21] cores) against doxorubicin (DOX), 6-hydroxydopamine (6-OHDA), and rotenone (ROT)-induced toxicity in C8-D1A astrocytes. In addition, dual-acting 5-HT$_6$R neutral antagonist/D$_3$R antagonist [22] also reduced the damage in C8-D1A cells exposed to DOX or 6-OHDA, respectively. Finally, a triple-acting 5-HT$_6$R neutral antagonist/5-HT$_3$R antagonist/MAO-B inhibitor effectively decreased the neuroinflammatory response triggered by the administration of Aβ_{25-35}, as assessed by the levels of reactive astrocytes and microglial markers (glial fibrillary acidic protein, GFAP; ionized calcium-binding adaptor molecule 1, Iba1) in the hippocampus [23].

In the present study, we report on a short series of 2-phenylpyrrole derivatives (Fig. 1) developed as a neutral antagonists at 5-HT$_6$R-operated Gs signaling. Through comparative analysis with previously disclosed 5-HT$_6$R ligands [24,25], and with the lead compound PZ-1388 [26], we demonstrate the relationship between the exposure of the basic center of the compounds and their ability to target specifically agonist-activated 5-HT$_6$R states. Finally, our study provides insights into the mechanisms underlying the cytoprotective properties of 5-HT$_6$R ligands in neurons and astrocytes including human-derived cells.

2. Chemistry

The synthetic route of the presented 5-HT$_6$R ligands is outlined in Scheme 1. The central 2-phenylpyrrole scaffolds (**1**–**8**) were obtained by Suzuki cross-coupling between 1-Boc-2-pyrroloboronic acid and iodobenzene derivatives, followed by NaOMe-mediated Boc deprotection. Then, coupling of alicyclic diamines to the central 2-phenyl ring was carried out by reductive amination to obtain secondary amine **9**, or Buchwald-Hartwig arylation to obtain tertiary amines **10**–**11**. The resulting compounds **9**–**11** reacted with sulfonyl chlorides in the presence of *tert*-butylimino-tri(pyrrolidino)phosphorane (BTPP) or *tert*-octylimino-tris(dimethylamino)phosphorane (P1-*t*-Oct) used as a proton scavenger. Another synthetic strategy was required for the introduction of alicyclic diamines to the terminal *N*-phenylsulfonyl ring. Sulfonylation of the pyrrole ring with 3-bromobenzenesulfonyl chloride or 3-fluorobenzenesulfonyl chloride provided compounds **12**–**18**, which underwent a copper-catalyzed Ullman reaction to obtain secondary amines **25**–**27**, or nucleophilic aromatic substitution to yield tertiary amines **28**–**33**. All the final products were obtained upon treatment with methanolic HCl to give the target compounds **19**–**33** as corresponding hydrochloride salts.

3. Results and discussion

3.1. Structure-activity relationship

Following the pharmacophore requirements [27], 2-phenylpyrrole was used as the aromatic hydrophobic fragment, enabling the introduction of a second hydrophobic site linked to the central scaffold by a sulfonyl group at the N^1 position of pyrrole as a hydrogen bond acceptor. In contrast to our previously reported 2-phenylpyrrole-3-carboxamides [25], the removal of the 3-carboxamide authorized changing the exposition of the basic center that was intended to be directly bound to the terminal aromatic fragments. The positively ionizable moiety was thus provided by the substitution of C^3 in the 2-phenyl ring (*Set 1*, compounds **19**–**24**) or C^3 in the *N*-phenylsulfonyl fragment (*Set 2*, compounds **25**–**33**) with selected alicyclic diamines. The affinity of the synthesized compounds **19**–**33** for 5-HT$_6$R was determined in the [^{3}H]-LSD binding assay using HEK293 cells stably expressing the human 5-HT$_6$Rs.

Set 1: The initial results showed that removing the 3-carboxamide fragment and shifting the basic center to the main aromatic core led to a two-fold decrease in affinity for 5-HT$_6$R compared to the prototype compound (**19** *vs* PZ-1388). Replacing a 4-piperidinylamine with a 1-methylpiperazinyl moiety resulted in a moderately active compound **21** while introducing an unsubstituted piperazinyl group did not affect the affinity for the target receptor (**19** *vs* **22**). In turn, decorating the *N*-phenylsulfonyl fragment with small-size halogens, namely fluorine or chlorine, was not favorable for binding to 5-HT$_6$R (**19** *vs* **20**; **22** *vs* **23**, **24**) (Table 1).

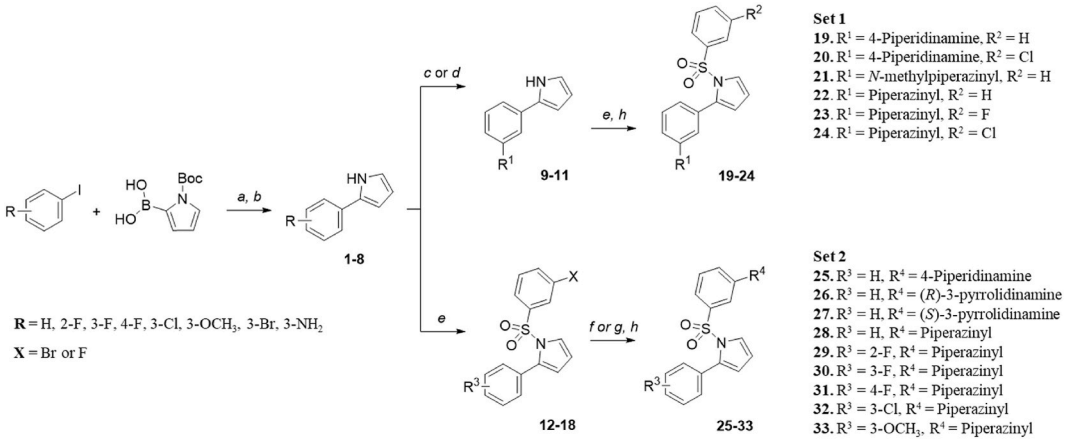

Scheme 1. General synthetic route for the preparation of final compounds **19**–**33**. **Reaction conditions:** *(a)* $Pd(PPh_3)_4$, K_2CO_3, 1,4-dioxane/H_2O, 90 °C, overnight; *(b)* NaOMe, MeOH, rt, overnight (55–86 %, two steps); *(c)* 1-Boc-4-piperidone, $NaBH(OAc)_3$, CH_2Cl_2, rt, 24 h (48 %); *(d)* 1-methyl-piperazine or 1-Boc-piperazine, $Pd_2(dba)_3$, 1,3-bis(2,6-diisopropylphenyl)-imidazolinium chloride, LHMDS in THF, 80 °C, 2 h, MW (75–81 %); (*e*) R^2PhSO_2Cl or X-$PhSO_2Cl$, BTTP or P_1-*t*-Oct, CH_2Cl_2, 0 °C to rt, 3 h (20–69 %); *(f)* 4-amino-1-Boc-piperidine, CuI, 2-acetylcyclohexanone, Cs_2CO_3, DMF, MW, 80 °C, 2 h (66–72 %); *(g)* piperazine, DMSO, 160 °C, 6 h or 180 °C, 2 h, MW, (26–57 %); (*h*) HCl in MeOH, rt, 24 h, (45–85 %).

Table 1
Binding data for compounds **19**–**33** for 5-HT_6 receptor.

Set 1		Set 2	
No	**K_i [nM]** [a]	**No**	**K_i [nM]** [a]
19	25 ± 3.8	**25**	4 ± 0.6
20	124 ± 19.8	**26**	4 ± 0.8
21	70 ± 13.2	**27**	8 ± 1.0
22	27 ± 5.5	**28**	1 ± 0.2
23	42 ± 4.9	**29**	2 ± 0.3
24	45 ± 8.3	**30**	1 ± 0.1
		31	4 ± 0.7
		32	2 ± 0.2
		33	1 ± 0.2

[a] Mean K_i values (±SEM) based on three independent binding experiments in HEK293 cells.

Set 2: The structural rearrangement, obtained by exposing a basic center linked to the C^3 position of the *N*-phenylsulfonyl fragment, increased the affinity of 4-piperidinamine-bearing analog **25** for 5-HT_6R three-fold compared to PZ-1388. Further reducing the size of the alicyclic amine did not affect the activity for (*R*)-3-pyrrolidinamine (**26**), while its *S* counterpart (**27**) was not favorable for binding to the receptor. Replacing the secondary amine with a tertiary one significantly increased the affinity of the molecule for 5-HT_6R, resulting in the potent compound **28**. Subsequently, introducing fluorine into the central 2-phenyl ring (**29**–**31**) did not impact the activity of the molecules. Finally, substituting the *meta* position of the 2-phenyl ring with chlorine (**32**) and a methoxy group (**33**) did not affect binding to 5-HT_6R.

3.2. Selectivity towards off-targets

Structurally diverse compounds showing the highest affinity for the 5-HT_6R (**22**, **25**, **28**, **30**, **33**) were primarily evaluated for related off-targets using radioligand binding assays. The tested derivatives exhibited high selectivity for the 5-HT_6R over other serotonin (5-HT_{1A}, 5-HT_{2A}, 5-HT_7) and dopamine (D_2) receptors (Table 2). Among the series, compound **30** displayed the highest affinity for 5-HT_6R (K_i = 1 nM) and the greatest selectivity over 5-HT_{2A} receptor. Therefore, compound **30** could serve as a molecular probe for exploring distinct pharmacological responses associated with selective interactions with 5-HT_6R.

Table 2
Binding data for compounds **22**, **25**, **28**, **30**, **33**, PZ-1388, and intepirdine for 5-HT_6, 5-HT_{1A}, 5-HT_{2A}, 5-HT_7, and D_2 receptors.

Compd	K_i [nM] [a]				
	5-HT_6 receptor	5-HT_{1A} receptor	5-HT_{2A} receptor	5-HT_7 receptor	D_2 receptor
22	27 ± 5.5	2473 ± 354	15860 ± 3159	1316 ± 185	2699 ± 319
25	4 ± 0.6	40610 ± 6591	1538 ± 264	1986 ± 371	10770 ± 2084
28	1 ± 0.2	755 ± 134	412 ± 77	12280 ± 2198	2174 ± 312
30	1 ± 0.1	1839 ± 237	2505 ± 459	11530 ± 1538	4334 ± 757
33	1 ± 0.2	916 ± 112	655 ± 93	11630 ± 1359	5199 ± 561
PZ-1388	12.6 ± 1	68610 ± 13359	10590 ± 1468	83960 ± 16624	7687 ± 1441
Intepirdine	1.3 ± 0.2	2370 [b]	25.1 ± 4	14230 [b]	997 [b]

[a] Mean K_i values (± SEM) based on three independent binding experiments in HEK293 cells for 5-HT_{1A}, 5-HT_6, 5-HT_7, D_2 receptors and CHO–K1 cells for 5-HT_{2A} receptor.
[b] Data was taken from Ref. [30].

3.3. Functional profiling at 5-HT_6R-operated Gs signaling

The effect of representative compounds from *Set 1* (**22**) and *Set 2* (**25**, **28**, **30**) on adenylate cyclase activity was examined in 1321N1 cells expressing 5-HT_6R using time-resolved fluorescence resonance energy transfer (TR-FRET) measurements using LANCE cAMP detection kit. For these experiments some reference inverse agonists at 5-HT_6R-operated Gs signaling (intepirdine; 2-(3-fluorophenyl)-1-[(3-chlorophenyl)sulfonyl]-*N*-(piperidin-4-yl)-1*H*-pyrrole-3-carboxamide, PZ-1388) [26], and a neutral antagonist at 5-HT_6R-operated Gs signaling ((*S*)-1-[(3-chlorophenyl)sulfonyl]-4-(pyrrolidine-3-yl-amino)-1*H*-pyrrolo [3,2-c] quinoline, CPPQ) [29] were used as controls. Despite the structural diversity around the central 2-phenylpyrrole framework, all of the new compounds inhibited 5-carboxamidotryptamine (5-CT)-stimulated cAMP accumulation and were classified as 5-HT_6R antagonists with K_b values ranging from 2.1 to 72.3 nM (Table 3).

The 5-HT_6R displays a high level of constitutive activity at Gs signaling in NG108-15 cells. Basal cAMP levels can be measured using a BRET-based probe (CAMYEL) [31], and the effect of compounds on

Table 3
Intrinsic activity and functional data at 5-HT$_6$ receptor-operated Gs signaling for selected compounds **22**, **25**, **28**, **30** and reference compounds (PZ-1388, intepirdine, CPPQ).

Compd	K_b [nM][a]	Functional profile at Gs[b]
22	72.3 ± 13.6	Neutral antagonist
25	16.2 ± 3.2	Neutral antagonist
28	2.1 ± 0.3	Neutral antagonist
30	4.7 ± 0.8	Neutral antagonist
PZ-1388	12.9 ± 1.6	Inverse agonist, IC_{50} = 164 nM
Intepirdine	1.5 ± 0.2	Inverse agonist, IC_{50} = 96 nM[c]
CPPQ	0.41 ± 0.06	Neutral antagonist[d]

[a] Mean K_b values (±SEM) based on three independent binding experiments in 1321N1 cells.
[b] Based on at least three independent experiments performed in triplicate in NG108-15 cells.
[c] Data are in line with Ref. [28].
[d] Data are in line with Ref. [29], where CPPQ is encoded as 14.

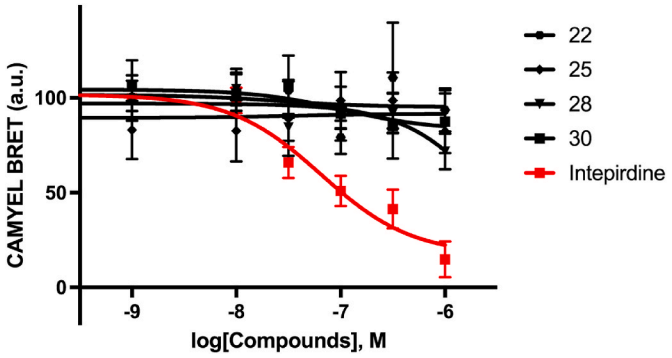

Fig. 2. Impact of compounds **22**, **25**, **28**, **30** and intepirdine on basal cAMP production in NG108-15 cells transiently expressing 5-HT$_6$Rs. Data are the mean ± SEM of the values obtained in at least three independent experiments performed in triplicate in different sets of cultured cells.

constitutive cAMP production can be quantified. This enables us to classify 5-HT$_6$R antagonists into neutral antagonists or inverse agonists. Selected compounds were further assessed in NG108-15 cells transiently expressing the CAMYEL probe and the 5-HT$_6$R [14,15]. Compounds **22**, **25**, **28**, **30** and CPPQ did not affect the basal cAMP level as assessed by bioluminescence resonance energy transfer (BRET) and were classified as neutral antagonists at Gs signaling. In contrast, intepirdine decreased the cAMP level in a concentration-dependent manner and behaved as 5-HT$_6$R inverse agonists (Fig. 2) as well as the prototypic molecule PZ-1388 (Fig. S1). These results suggest that removing the 3-carboxamide moiety and shifting the basic center provides compounds that target different conformational states of 5-HT$_6$R than previously reported 2-phenylpyrrole-3-carboxamide derivatives (e.g., PZ-1388) [24,25].

3.4. Molecular modeling

The serotonin-bound human 5-HT$_6$R-Gs heterotrimer [32] provides an intriguing tool for developing ligands targeting different active states of the receptor and thus impact its interactome. To gain deeper insight into the impact of exposing the basic center on binding mode and receptor affinity, we assessed the molecular mechanism of action for structurally distinct compounds, PZ-1388 (reference inverse agonist) [26], CPPQ (reference neutral antagonist) [29], **22** and **28,** using an induced-fit docking (IFD) approach to the 5-HT$_6$R crystal structure (PDB ID: 7XTB). The binding mode of CPPQ was consistent with our previously published findings [20,23]. In PZ-1388, the protonated piperidine moiety forms a salt bridge (SB) with D3x32. The *N*-sulfonylpyrrole moiety engages with N6x56 and extracellular loop 2 (ECL2) with L45x52 *via* hydrogen bonds (HBs). Furthermore, the terminal substituted phenyl ring fits into a hydrophobic pocket framed by transmembrane domains (TMs) **3**–**5**, establishing a halogen bond (XB) with A4x56 (Fig. 3A). However, the binding modes revealed by IFD did not explain the different functional profiles at Gs signaling for compounds PZ-1388 and CPPQ. Therefore, we conducted a series of 100 ns-long molecular dynamics (MD) simulations, utilizing geometries pinpointed in the IFD analysis. Subsequent clustering of the MD trajectories identified the five most prevalent geometries for further examination. The MD insights revealed that while PZ-1388 and CPPQ maintain crucial ligand–receptor (L–R) interactions (D3x32, A4x56, F5x38, F6x51, N6x56, and Y7x42), they also induce notable alterations in the receptor's structure. The analysis of the geometric center shifts (Δd) in individual amino acids highlighted marked differences in the conformations of the PZ-1388- and CPPQ-receptor complexes. The most pronounced alterations (exceeding 4 Å) were observed in the binding pocket (areas highlighted in pink on the helix graphs), particularly in TMs **5**–**6**. Meanwhile, changes in the other TMs were generally below 4 Å, except for four amino acids in TM3, which lack direct interaction with the ligands (Fig. 3B). It is worth stressing that interacting amino acids show almost the lowest Δd.

To ascertain if comparable variations in binding modes and molecular dynamics are observed, compounds **22** and **28** were further analyzed. While both molecules established an SB with D3x32, they occupied slightly different spaces within the binding pocket (Fig. 4A and B). The *N*-phenylpiperazine fragment of **22** took up a position similar to the 3-fluorophenyl group in PZ-1388, while the sulfonyl-1*H*-pyrrole replaced the terminal 3-chlorophenyl. Additionally, the *N*-phenylsulfonyl group formed an N–H···π hydrogen bond (HB) with N6x56 (Fig. 4A). Despite compound **22** exhibiting nanomolar activity, the lack of interaction with TM4 could potentially lead to less optimal values. In turn, compound **28** demonstrates a different binding spatial arrangement and interaction pattern within the receptor compared to **22**. The

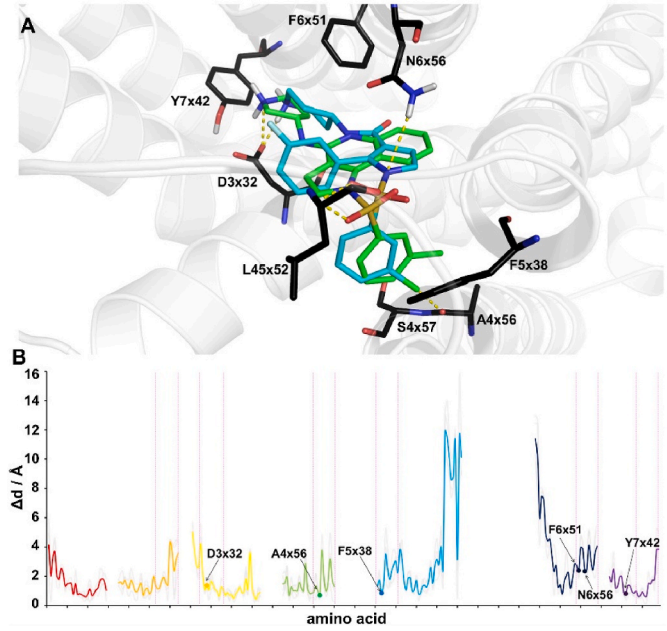

Fig. 3. (**A**) Comparison of the binding modes of CPPQ (green) and PZ-1388 (cyan) in the binding pocket of 5-HT$_6$R, based on the most populated MD clusters. (**B**) Plot demonstrating the link between the geometric center's position of a specific amino acid (Δd), calculated as the average deviation between conformations of PZ-1388 and CPPQ from the clustered MD trajectory. The pink lines marks segments of the helix sequence, indicating amino acids that constitute the receptor's active site. Amino acids are encoded using GPCRdb residue numbering scheme, an extension of the Ballesteros-Weinstein system [33].

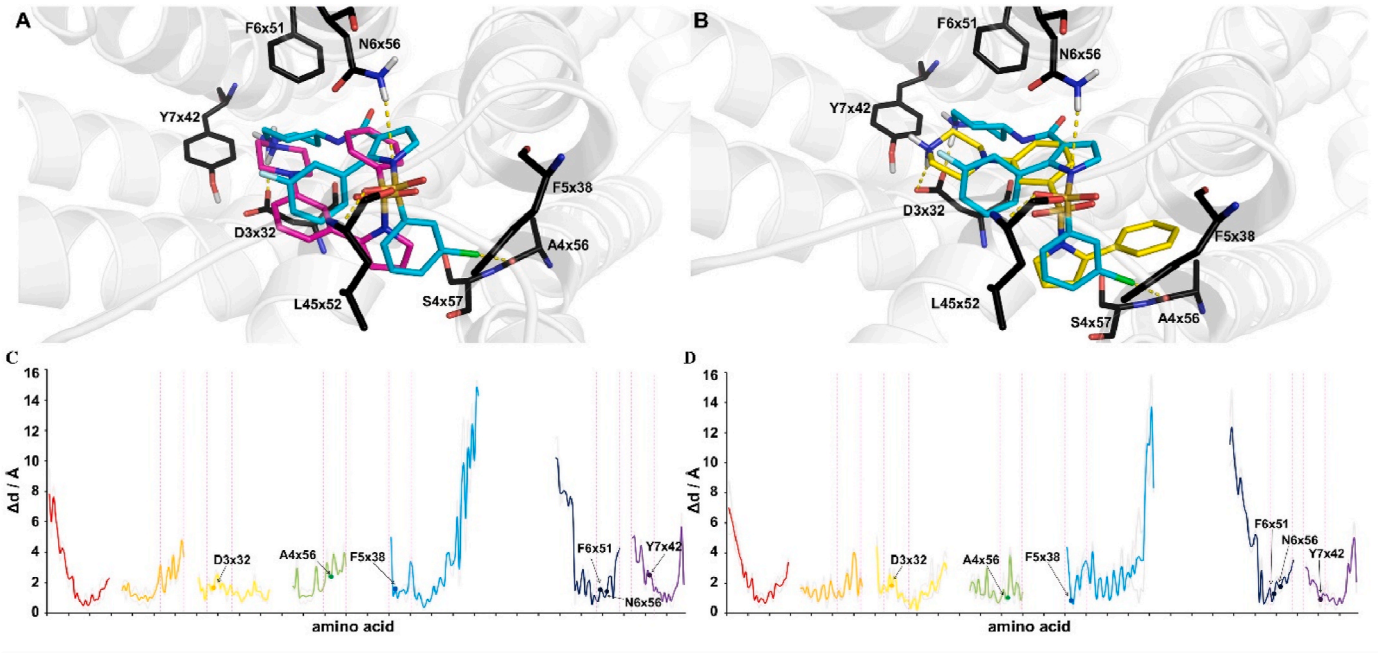

Fig. 4. Comparison of the binding modes of (**A**) PZ-1388 (cyan) and **22** (magenta) or (**B**) PZ-1388 (cyan) and **28** (yellow) in the binding pocket of 5-HT$_6$R, based on the most populated MD clusters. Plots demonstrating the link between the geometric center's position of a specific amino acid, calculated as the average deviation between conformations of (**C**) PZ-1388 and **22**, or (**D**) PZ-1388 and **28** from the clustered MD trajectory. Additionally, the pink lines marks segments of the helix sequence, indicating amino acids that constitute the receptor's active site.

phenyl-1*H*-pyrrole fragment of **28** is positioned in stark contrast to PZ-1388, lying correctly in the opposite section of the binding pocket. This distinct replacement highlights the diverse ways of interacting with the receptor while still maintaining the key interactions. The terminal phenyl fragment extends towards a hydrophobic cavity encompassed by transmembrane domains (TMs 4–5), engaging in a π···π interaction with F5x38 and alone pair···π interaction with A4x45 (Fig. 4B). In the case of compound **30**, fluorine substitution of C^3 in the 2-phenyl ring, did not affected the binding mode (Fig. S2A): it only enhanced the π···π interaction with F5x38 due to the increased acidity of the aromatic hydrogens [34].

To explain the differences in functional profile at Gs signaling, we further replicated the MD approach for PZ-1388 and developed compounds **22** and **28**. The results present the conformational changes in TM5 and TM6 as primarily responsible for the differences in the biological functions and signal transduction of the ligands (Fig. 4C, **D**). Interestingly, the key residues interacting with the compounds exhibited minimal changes (less than 4 Å). In addition, the simulations revealed no significant changes in the position of TM helices in case of **28** and its fluorinated analogue **30** (Fig. S2B). Furthermore, when comparing the simulation clusters of **22** and **28** with CPPQ, they did not exhibit similar profiles of changes (Fig. S3). This alignment with earlier studies reinforces the critical role of TM5 and TM6 in dictating ligand functionality and the receptor's signal transduction pathways [20,23,35]. These findings collectively emphasize the importance of considering the dynamic conformational changes of these transmembrane domains in understanding ligand-receptor interactions and their subsequent impact on biological function.

3.5. Functional profiling at 5-HT$_6$R-operated Cdk5 signaling

Agonist-independent activation of Cdk5 by 5-HT$_6$R plays a key role in the initiation of neurite growth and the migration of cortical neurons [15,16] Preventing the Cdk5-mediated phosphorylation of the 5-HT$_6$R with receptor's inverse agonists inhibits neurite growth, while neutral antagonists do not impact this process. Transfection of 5-HT$_6$R in NG108-15 cells resulted in a significant increase in neurite length compared with yellow fluorescent protein (YFP)-transfected cells (Fig. 5). The most promising compounds **28** and **30**, applied at a concentration of 10 nM, significantly reduced the neurite length and were classified as full inverse agonists at 5-HT$_6$R-operated Cdk5 signaling, in line with intepirdine used as a reference. Notably, these molecules showed an exceptional functional profile: while stabilizing the 5-HT$_6$R constitutive activity at the Gs pathway, they remained capable of inhibiting Cdk5 signaling.

3.6. Preliminary in vitro ADME/Tox assesment

Preliminary pharmacokinetics characterization, reflecting dynamic interactions between a biological system and drug-like molecules, provides critical assessments in lead selection. In the first step, we used a computational approach to assess central nervous system multiparameter optimization (CNS MPO) [36]. The calculated values of CNS MPO ranged between 3.98 and 5.30, indicating similar ADME attributes, which are adequate for drug-like molecules targeting the central nervous system (Table S1). Further biotransformation studies of the most promising compounds **22**, **25**, **28**, **30** and **33** were evaluated using rat liver microsomes (RLMs). A higher value of intrinsic clearance was observed for derivative **22**, bearing a basic center, piperazinyl moiety, introduced to the central 2-phenyl ring. In turn, compounds **25**, **28**, **30** and **33**, with alicyclic diamines in the terminal *N*-phenylsulfonyl ring, exhibited high to moderate metabolic stability (Cl_{int} < 50 μL/min/mg) (Table 4). The most promising derivative **30** was also evaluated for safety-related off-targets effects. It was found that **30** does not block the *h*ERG potassium channel (8 % at 1 μM) and displays acceptable affinity towards H_3 (14.5 % at 1 μM), D_3 (63.3 % at 1 μM), and σ_1 (75.5 % at 1 μM) receptors compared to its high affinity at 5-HT$_6$R (K_i 5HT$_6$R = 1 nM). However, compound **30** inhibited the activity of the 3A4 isoform of cytochrome P450 (94 % at 10 μM), which might impact drug–drug interactions. In addition, compound **30** did not induce any significant cytotoxic effect at concentration range related to its effect on 5-HT$_6$R as assessed in neuroblastoma SHSY-5Y (IC_{50} = 18.5 μM),

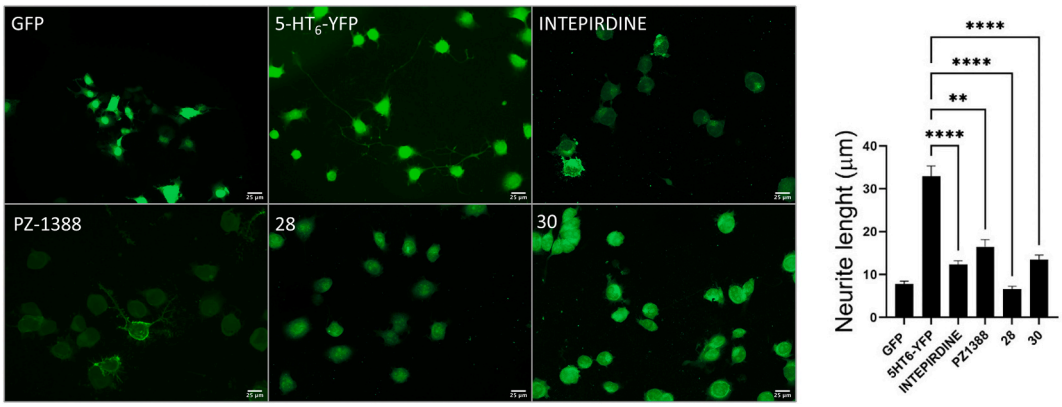

Fig. 5. Impact of intepirdine, PZ-1388, **28** and **30** on Cdk5 signaling pathway. NG108-15 cells were transfected with a plasmid encoding a YFP tagged 5-HT_6R or YFP alone. Cells expressing the receptor were exposed to DMSO (vehicle), intepirdine, PZ-1388, **22** and **30** (10^{-8} M) for 24 h. The histogram shows the mean ± SEM of neurite length for each experimental condition measured from three independent experiments: $^{**}P < 0.006$, $^{****}P < 0.0001$ *vs* cells treated with vehicle; ANOVA followed by Tukey's multiple comparison test.

Table 4
Metabolic stability of selected compounds in rat liver microsomes.

Compd	$t_{1/2}$ [min]	Cl_{int} (µL/min/mg)[a]	Major metabolic pathway[b]
22	15.3	109.1	Hydroxylation
25	101.1	20.6	Hydroxylation
28	83.6	24.9	Hydroxylation
30	49.3	32.4	Not detected
33	36.7	56.7	Not detected
Imipramine	15.9	104.1	*N*-demethylation

[a] Determined in the RLM test, at a protein concentration of 0.5 mg/mL.
[b] Assessed by UPLC/MS analysis. Results are means of two independent experiments run in duplicate.

pheochromocytoma PC-12 (IC_{50} = 25.6 µM), astrocytes C8-D1A (IC_{50} = 37.4 µM), and human astrocytes (IC_{50} = 39.3 µM) (Table S2).

3.7. *Cytoprotective activity of 5-HT$_6$R neutral antagonists*

Although the expression of 5-HT_6R in various neuronal and glial populations is well documented [20,37,38], the data concerning the impact of 5-HT_6R constitutive activity on cellular processes remains limited. To explore the potential cytoprotective effect of 5-HT_6R modulators on neurons and astrocytes, we selected compounds exhibiting different functional profiles at 5-HT_6R-operated Gs signaling: 5-HT_6R agonist (WAY-208466), nonselective 5-HT_6R inverse agonist (intepirdine), 5-HT_6R selective inverse agonist (PZ-1388), 5-HT_6R neutral antagonist (CPPQ), and evaluated them together with newly developed compounds **22**, **28** and **30**. In the initial step, selected compounds were tested in two cellular models of exposition to damaging factors typical for neurodegenerative diseases. We used human neuroblastoma (SHSY–5Y) exposed to 6-hydroxydopamine (6-OHDA) to model Parkinson's disease, and rat pheochromocytoma (PC12) exposed to β-amyloid ($A\beta_{25-35}$) to recreate damages observed in Alzheimer's disease. In both experimental models, only CPPQ produced a significant neuroprotective effect increasing the viability of cells damaged by neurotoxins, as assessed in the cellular metabolic activity MTT test. Such an effect was not observed in the presence of compounds **22**, **28**, **30**, and remarkably also by molecules displaying either agonist (WAY-208466) or inverse agonist (intepirdine, PZ-1388) properties at 5-HT_6R-operated Gs signaling (Fig. 6A, **B**).

Since astrocytes play a crucial role in maintaining brain homeostasis and initiating the cell repair system [39], prevention of their damage represents a holistic approach in neuroprotection studies. Threfore, we evaluated the impact of the presented 5-HT_6R ligands on glial cells damages using a further model, the C8-D1A cells exposed to rotenone

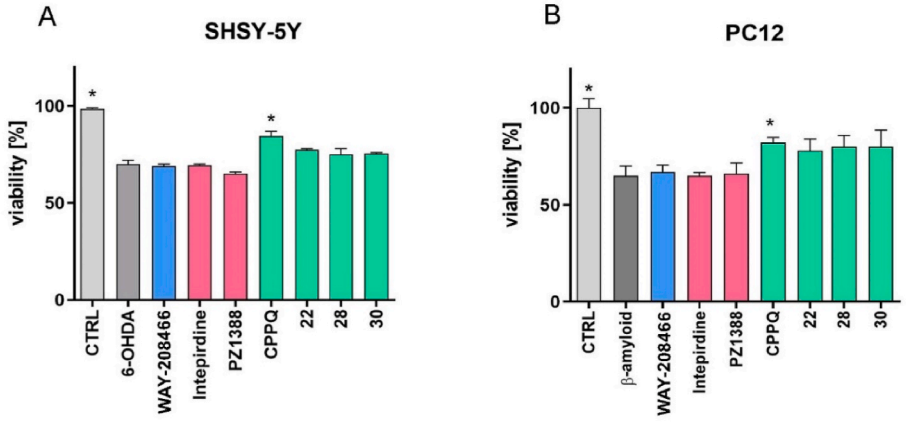

Fig. 6. (**A**) CPPQ, but not compounds **22**, **28**, **30,** WAY-208466, intepirdine, or PZ-1388 reduce 6-OHDA-induced cytotoxicity in SHSY-5Y cells assessed in MTT assay. (**B**) CPPQ, but not compounds **22**, **28**, **30,** WAY-208466, intepirdine, or PZ-1388 reduce β-amyloid induced cytotoxicity in PC12 cells assessed in MTT assay. Cells were incubated in the presence of analyzed compounds for 3 h (0.25 µM), then the culture medium was aspirated and changed to fresh, containing: 6-OHDA-20 µM or β-amyloid-2.5 µM, respectively, for the next 24 h. Then, an MTT assay was performed to assess the metabolic activity of cells. The histograms represent the mean viability of cells ± SEM. N = 12, $^{*}p < 0.05$, statistical significance was determined using the Brown–Forsythe and Welch's ANOVA tests, along with the post-hoc unpaired *t*-test with Welch's correction.

(ROT). The molecules displaying neutral antagonists properties (CPPQ, **22**, **28**, **30**) significantly increased astrocyte viability in the MTT test as well as decreased the cytotoxic effect in the CytoTox-Glo test assay, which determines cell membrane integrity. In contrast, the 5-HT_6R agonist (WAY-208466) and inverse agonists (intepirdine, PZ-1388) did not induce any protective effect (Fig. 7A, **B**). Due to some limitations in translating the results obtained in animal and human cells, we further assessed the protective activity of selected compounds using human-derived astrocytes. Preincubation of astrocytes with all neutral antagonists (CPPQ, **22**, **28**, **30**) led to a remarkable reduction in cellular damage induced by rotenone, as indicated in MTT and CytoTox-Glo tests (Fig. 7C, **D**). A similar effect was observed when exposing human astrocytes to 6-OHDA (Fig. S4). Notably, compounds that exhibit agonist or inverse agonist properties did not produce glioprotection.

Finally, the impact of compound **30** on human-derived astrocyte cytoskeleton was evaluated using fluorescent microscopy. Extended preincubation of the cells with **30** prevented damage of the actin cytoskeleton caused by stress factors such as 6-OHDA and rotenone (Fig. 8). These results suggest that the glioprotective mechanism of compound **30** is complex and based not only on the improvement of mitochondrial performance and cell membrane conditions but also on processes affecting the cytoskeleton, which is crucial in cell physiology.

4. Conclusions

Herein, we extended our studies on the contribution of active states of 5-HT_6R to cytoprotective effects in mice and human astrocytes. Starting from previously reported 2-phenyl-1*H*-pyrrole-3-carboxamide-based 5-HT_6R inverse agonists, we developed novel neutral antagonists at 5-HT_6R-operated Gs signaling. Systematic structure–activity relationship studies indicated the exposition of the compound's basic center in the terminal sites of the central phenylsulfonamides of the 2-phenylpyrrole framework as a crucial feature that impacts the functional profile at Gs signaling. This was further confirmed in molecular dynamics simulations showing conformational changes in TM5 and TM6 as structural determinant characteristics for 5-HT_6R neutral antagonists at Gs signaling. The study identified compound **30**, a potent and selective ligand that behaves as a neutral antagonist at 5-HT_6R-operated Gs signaling and an inverse agonist at the Cdk5 pathway. We demonstrated the cytoprotective effects of neutral antagonists at 5-HT_6R-operated Gs signaling, particularly towards C8-D1A and human astrocytes. The effect was directly correlated to the compound's activity at Gs signaling but not the chemical structure. In line with our previous studies [20,21,23], all the tested neutral antagonists at 5-HT_6R-operated Gs signaling (**22**, **28**, **30**, CPPQ), but neither the 5-HT_6R agonist (WAY-208466) nor the 5-HT_6R inverse agonists (intepirdine, PZ-1388), produced the protective effect. Our results outline 2-phenyl-1*H*-pyrrole as an interesting framework for 5-HT_6R ligands and provide valuable molecular probes to

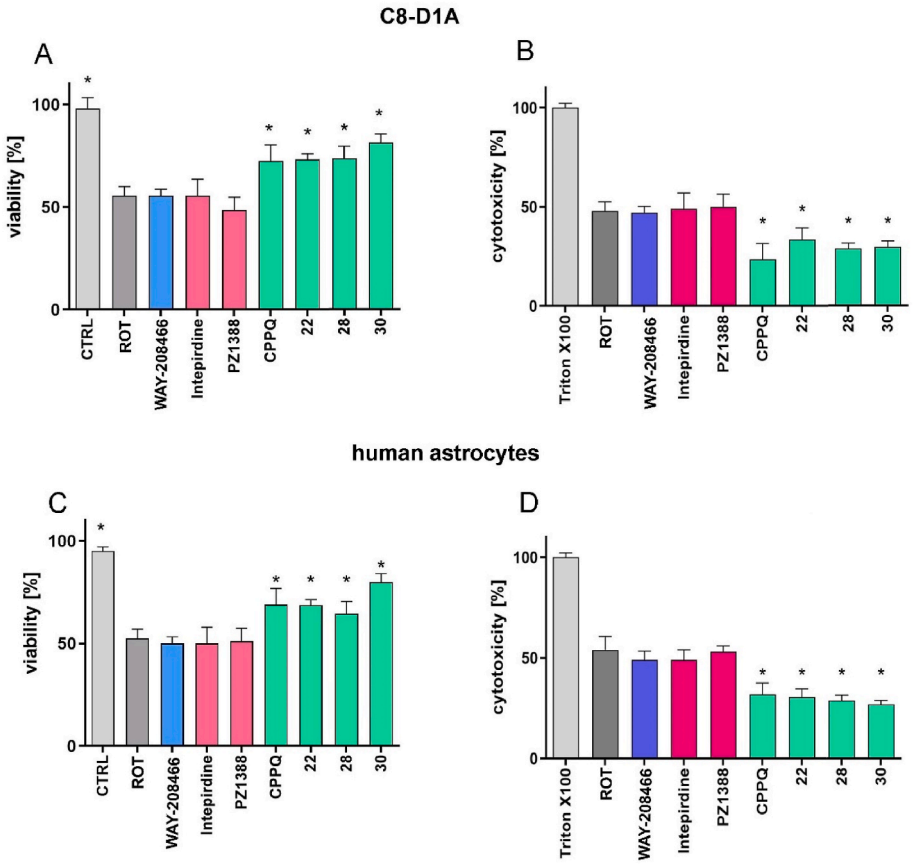

Fig. 7. (**A**) Compounds **22**, **28**, **30** and CPPQ, but not WAY-208466, intepirdine, or PZ-1388 reduce ROT-induced cytotoxicity in C8-D1A astrocytes assessed in MTT assay. (**B**) Compounds **22**, **28**, **30** and CPPQ, but not WAY-208466, intepirdine, or PZ-1388 reduce ROT-induced cytotoxicity in C8-D1A astrocytes assessed in CytoTox-Glo assay. (**C**) Compounds **22**, **28**, **30** and CPPQ, but not WAY-208466, intepirdine, or PZ-1388 reduce ROT-induced cytotoxicity in human astrocytes assessed in MTT assay. (**D**) Compounds **22**, **28**, **30** and CPPQ, but not WAY-208466, intepirdine, or PZ-1388 reduce ROT-induced cytotoxicity in human astrocytes assessed in CytoTox-Glo assay. Cells were incubated in the presence of analyzed compounds for 3 h (0.25 μM), then the culture medium was aspirated and changed to fresh, containing ROT (0.5 μM) for the next 24 h. Then, MTT or CytoTox-Glo assay was performed to assess the cellular metabolic condition or cell membrane integrity, respectively. The histograms represent the mean viability of cells (MTT) or cytotoxicity (CytoTox-Glo) ± SEM. N = 12, $^*p < 0.05$, statistical significance was determined using the Brown–Forsythe and Welch's ANOVA tests, along with the post-hoc unpaired *t*-test with Welch's correction.

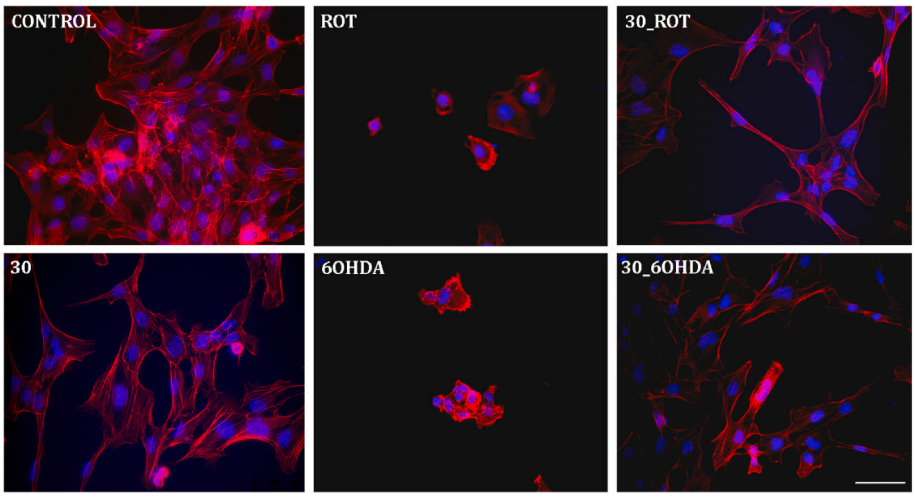

Fig. 8. Effect of compound **30** on cytoskeleton organization in human astrocytes damaged with 6-OHDA or ROT Cells were incubated in the presence of analyzed compounds for 3 h (0.25 μM), then culture medium was aspirated and changed to fresh, containing ROT (0.5 μM) or 6-OHDA (20 μM) for next 24 h. Next, actin cytoskeleton and cell nuclei staining were performed as described in the material and methods section. Pictures were taken using a Leica DMiL LED Fluo microscope equipped with LAS-X Software (40× objective), scale bar = 50 μm.

develop potential therapies targeting the agonist-activated state of 5-HT_6R.

5. Experimental methods

5.1. Chemistry

Commercially available reagents and solvents were used as provided by the suppliers without further purification. Moisture-sensitive processes were carried out under an atmosphere of nitrogen using anhydrous solvents. Microwave-assisted reactions were conducted in Initiator$^+$ microwave synthesizer Biotage®. Reaction progress was monitored by thin-layer chromatography (TLC) and/or high-performance liquid chromatography (HPLC). HPLC conversion was measured using (*a*) Arc Waters System equipped with a UV/Vis Waters 2998 PDA spectrophotometric detector using a Chromolith SpeedROD RP-18 50 × 4.6 mm column and a linear gradient from 0 to 95 % CH_3CN/0.1 % HCOOH in H_2O/0.1 % HCOOH over 3 min, detection at 214 nm, flow rate: 3 mL min^{-1}; or (*b*) Agilent Technologies 1220 Infinity LC using a Chromolith high-resolution RP-18e 50 × 4.6 mm column and a linear gradient of 0–100 % CH_3CN/0.1 % TFA in H_2O/0.1 % TFA over 3 min, detection at 214 nm. Flow rate: 1 mL min^{-1}. Crude products were purified using silica gel Merck 60 (70–230 mesh), flash chromatography using a Biotage® Isolera™ system with SNAP HP-Sil cartridges, or preparative reverse-phase HPLC methodology with UV detection. The fractions obtained were concentrated under reduced pressure to remove organic volatiles. Mass spectra were recorded on a UPLC–MS/MS system consisting of q Waters Acquity I-Class Plus coupled to a Waters Synapt XS mass spectrometer (electrospray ionization mode ESI). Chromatographic separations were carried out using the Acquity UPLC BEH (bridged ethylene hybrid) C18 column; 100 × 2.1 mm, equipped with Acquity UPLC BEH C18 VanGuard pre-column; 5 × 2.1 mm and a linear gradient from 0 to 95 % CH_3CN/0.1 % HCOOH in H_2O/0.1 % HCOOH over 10 min, flow rate: 3 mL min^{-1}. Chromatograms were recorded using Waters eλ PDA detector; spectra were analyzed in the 200–700 nm range with 1.2 nm resolution and a sampling rate of 20 points/s. Retention times, t_R, were given in minutes. The UPLC/MS purity of all the final compounds and key intermediates was confirmed to be 95 % or higher. ^{1}H NMR, ^{13}C NMR, ^{19}FNMR spectra were recorded with Varian BB 200 (300 and 75 MHz), Bruker Avance III (400 MHz and 101 MHz) or JEOL JNMECZR 500 RS1 (500, 471, and 126 MHz) and are reported in ppm using deuterated solvent for calibration ($CDCl_3$, CD_3OD or DMSO-d_6). The *J* values are reported in hertz (Hz), and the splitting patterns are designated as follows: br s (broad singlet), s (singlet), d (doublet), t (triplet), q (quartet), dd (doublet of doublets), dt (doublet of triplets), td (triplet of doublets), ddd (doublet of doublets of doublets), m (multiplet). Elemental analyses for C, H, and N were carried out using the elemental Vario EL III Elemental Analyser.

The synthetic procedures and description of the final compounds **19**–**33** are presented below. Characterization data for the intermediate compounds **1**–**18** are presented in the Supporting **Information**.

5.1.1. General procedures for the synthesis of compounds *1*–*33*

General procedure 1: Suzuki–Miyaura cross-coupling (**1**–**8**): The appropriate aryl iodide (1 eq), *N*-Boc-2-pyrroleboronic acid (1.3 eq), and K_2CO_3 (3 eq) were dissolved in the mixture of 1,4-dioxane and water (4/1, *v*/*v*). Under a constant flow of N_2, tetrakis(triphenylphosphine) palladium (0.05 eq) was subsequently added and the reaction mixture was stirred at 80 °C overnight. After cooling to ambient temperature, the mixture was diluted with EtOAc, filtered through celite and washed twice with H_2O and brine, dried over Na_2SO_4, and concentrated. Next, the crude product was dissolved in methanol and freshly prepared (from NaH and MeOH) NaOMe solution (~1 N in MeOH, 5 eq) was added, and the mixture was left to react overnight. Then, methanol was evaporated and the residue was dissolved in EtOAc, washed with H_2O and brine, dried over Na_2SO_4, and concentrated. The crude product was purified on silica gel (the eluting system is indicated for each compound together with characterization data).

General procedure 2: Reductive amination (**9**): 3-(1*H*-pyrrol-2-yl) aniline (1 eq) and 1-Boc-4-piperidone (1.5 eq) were dissolved in CH_2Cl_2, followed by the addition of sodium triacetoxyborohydride (1.5 eq). The mixture was stirred at rt overnight, and an additional portion of 1-Boc-4-piperidone (0.5 eq) and sodium triacetoxyborohydride (0.5 eq) were added and left to react for 5 h. Then, water and 10 mL of 1 N NaOH were added and the reaction was extracted twice with DCM. The organic phases were combined and washed with brine, dried over $MgSO_4$, concentrated, and purified on silica gel (the eluting system is indicated together with characterization data).

General procedure 3: Buchwald-Hartwig amination (**10**–**11**): An oven-dried microwave vial was charged with 2-(3-chlorophenyl)-1*H*-pyrrole **4** (1 eq), an amine (2 eq), $Pd_2(dba)_3$ (0.1 eq), 1,3-bis(2,6-diisopropylphenyl)-imidazolinium chloride (SIPr*HCl) (0.1 eq) and a magnetic stirrer bar and then sealed with a septum. The vial was evacuated and backfilled with nitrogen three times, after which anhydrous THF

and LHMDS (1 M solution in THF, 5 eq) were added. Next, the reaction was stirred at 80 °C for 2 h under microwave irradiation. After cooling down, the mixture was diluted with EtOAc, filtered through celite, washed twice with H_2O and brine, and dried over Na_2SO_4. The solvent was removed under reduced pressure and the crude product was purified by flash column chromatography (the eluting system is indicated for each compound together with characterization data).

General procedure 4: Sulfonylation (**12**–**24**): The pyrrole derivative **1**–**11** (1 eq) was dissolved in CH_2Cl_2 and cooled down to 0 °C (for the synthesis of **12**−**18** and **21**−**24)** or −78 °C (for the synthesis of **19**, **20**), followed by addition of phosphazene base P_1-*t*-Bu-tris(tetramethylene) (for the synthesis of **12**, **14**, **17**−**24**, 1.5 eq) or *tert*-octylimino-tris (dimethylamino)phosphorane) (for the synthesis of **13**, **15**, **16**, 1.5 eq). Then the appropriate sulfonyl chloride (1.5 eq) was added portion-wise within 2 h, and the reaction mixture was stirred at rt for an additional 3 h. The solvent was subsequently evaporated under reduced pressure and the remaining crude product was purified on silica gel or by using the preparative reverse-phase HPLC method (the method and eluting system are indicated for each compound together with characterization data).

General procedure 5: Ullman coupling (**25**–**27**): An oven-dried microwave vial was charged with a magnetic stirring bar, CuI (0.1 eq), Cs_2CO_3 (2 eq), and 4-amino-1-Boc-piperidine (for the synthesis of **25**, 2 eq). The vial was sealed, evacuated and backfilled with nitrogen. At this point anhydrous DMF and any remaining liquid materials: aryl bromide **12** (dissolved in anhydrous DMF), (*R*) or (*S*) 3-amino-1-Boc-pyrolidine (for the synthesis of **26**−**27**, 2 eq) and 2-acetylcyclohexanone (0.4 eq) was added. The reaction mixture was heated at 80 °C for 4 h and then cooled down, diluted with EtOAc, filtered through celite, washed with water and brine, dried over Na_2SO_4, and concentrated. The residue was purified on silica gel (the eluting system is indicated for each compound together with characterization data).

General procedure 6: Nucleophilic aromatic substitution (**28**–**33**): In a microwave vial or round bottom flask, the appropriate N^1-3-fluorophenylsulfonyl derivative **13**−**18** (1 eq) was dissolved in DMSO followed by the addition of piperazine (4 eq). Next, the reaction was stirred at 180 °C for 2 h under microwave irradiation (for **28**, **30**, **32**) or at 160 °C overnight (for **29**, **31**, **33**). After cooling to ambient temperature, the mixture was diluted with EtOAc and washed three times with H_2O (containing a few drops of ammonia) and brine, dried over Na_2SO_4, and concentrated. The residue was purified on silica gel (the eluting system is indicated for each compound together with characterization data).

All the final molecules, obtained as a Boc-protected or free bases, were dissolved in anhydrous ethanol, treated with 1.25 M methanolic HCl and stirred for 24 h to yield the final products as hydrochloride salts after evaporation.

5.1.2. Characterization data for final compounds ***19***−***33***

5.1.2.1. *N-(3-(1-(Phenylsulfonyl)-1H-pyrrol-2-yl)phenyl)piperidin-4-amine (**19**)*.

Following general procedure 1, 2, 4. **Boc-derivative:** yellow oil, 0.028 g (yield 20 %) after flash chromatography purification over silica gel (EtOAc 0−30 % in Hex); UPLC/MS purity 100 %, t_R = 9.01, $C_{26}H_{31}N_3O_4S$, MW 681.61, Monoisotopic Mass 481.20, $[M+H]^+$ 482.2. **Dihydrochloride hydrate**: creamy solid, 0.011 g (yield 45 %) after preparative chromatography purification using Luna Phenyl-Hexyl column (CH_3CN 5−90 % in H_2O with 0.1 % HCl) and lyophilization; UPLC/MS purity 100 %, t_R = 5.31, MW 472.43. ^{1}H NMR (400 MHz, CD_3OD) δ ppm 2.09 (qd, J = 12.8, 3.9 Hz, 2H), 2.31 (d, J = 13.7 Hz, 2H), 3.08−3.19 (m, 2H), 3.58 (d, J = 12.9 Hz, 2H), 3.97 (tt, J = 11.5, 3.9 Hz, 1H), 6.36 (dd, J = 3.1, 1.6 Hz, 1H), 6.42 (t, J = 3.1 Hz, 1H), 7.29 (dt, J = 6.3, 2.0 Hz, 1H), 7.37−7.41 (m, 2H), 7.42−7.48 (m, 2H), 7.52 (dd, J = 3.1, 1.6 Hz, 1H), 7.54−7.60 (m, 3H), 7.60−7.65 (m, 1H). Monoisotopic Mass: 381.15, $[M+H]^+$ 382.2. Elemental analysis calculated for $C_{21}H_{23}N_3O_2S\bullet 2HCl\bullet H_2O$ C: 53.39 %, H: 5.76 %, N: 8.89 %; found C: 53.17 %, H: 5.96 %, N: 8.96 %.

5.1.2.2. *N-(3-(1-((3-Chlorophenyl)sulfonyl)-1H-pyrrol-2-yl)phenyl)piperidin-4-amine (**20**)*.

Following general procedure 1, 2, 4. **Boc-derivative:** yellow oil, 0.036 g (yield 24 %) after flash chromatography purification over silica gel (EtOAc 0−30 % in Hex); UPLC/MS purity 96 %, t_R = 9.25, $C_{26}H_{30}ClN_3O_4S$, MW 516.05, Monoisotopic Mass 516.16, $[M+H]^+$ 517.2. **Dihydrochloride hydrate**: creamy solid, 0.016 g (yield 51 %); after preparative chromatography purification using Luna Phenyl-Hexyl column (CH_3CN 5−90 % in H_2O with 0.1 % HCl) and lyophilization; UPLC/MS purity 100 %, t_R = 5.74, MW 506.87. ^{1}H NMR (400 MHz, CD_3OD) δ ppm 2.01−2.14 (m, 2H), 2.35 (d, J = 12.9 Hz, 2H), 3.12−3.23 (m, 2H), 3.61 (d, J = 12.9 Hz, 2H), 3.96 (ddd, J = 11.1, 7.3, 3.9 Hz, 1H), 6.41 (dd, J = 3.3, 1.8 Hz, 1H), 6.48 (t, J = 3.3 Hz, 1H), 7.21 (d, J = 7.4 Hz, 1H), 7.34 (t, J = 2.0 Hz, 1H), 7.38−7.42 (m, 1H), 7.47−7.54 (m, 3H), 7.57 (dt, J = 3.5, 1.8 Hz, 2H), 7.69 (dt, J = 6.9, 1.1 Hz, 1H). Monoisotopic Mass: 415.11, $[M+H]^+$ 416.1. Elemental analysis calculated for $C_{21}H_{22}ClN_3O_2S\bullet 2HCl\bullet H_2O$ C: 49.76 %, H: 5.17 %, N: 8.29 %; found C: 50.05 %, H: 5.36 %, N: 8.48 %.

5.1.2.3. *1-Methyl-4-(3-(1-(phenylsulfonyl)-1H-pyrrol-2-yl)phenyl)piperazine (**21**)*.

Following general procedure 1, 3, 4. **Free base:** yellow oil, 0.110 g (yield 54 %) after flash chromatography purification over silica gel (EtOAc 30−80 % in Hex); UPLC/MS purity 100 %, t_R = 4.85, $C_{21}H_{23}N_3O_2S$, MW 381.49, Monoisotopic Mass 381.15, $[M+H]^+$ 382.2. **Dihydrochloride hydrate**: brown solid, 0.070 g (yield 58 %), UPLC/MS purity 100 %, t_R = 4.87, MW 472.43. ^{1}H NMR (500 MHz, CD_3OD) δ ppm 2.95 (s, 3H), 3.08 (br. s, 2H), 3.26 (br. s, 2H), 3.58 (br. s, 2H), 3.78 (br. s, 2H), 6.17 (dd, J = 3.4, 1.7 Hz, 1H), 6.33 (t, J = 3.4 Hz, 1H), 6.64–6.68 (m, 1H), 6.86 (dd, J = 2.3, 1.4 Hz, 1H), 7.02 (ddd, J = 8.3, 2.6, 0.9 Hz, 1H), 7.18 (t, J = 7.7 Hz, 1H), 7.29–7.33 (m, 2H), 7.34–7.39 (m, 2H), 7.46 (dd, J = 3.3, 1.9 Hz, 1H), 7.54–7.59 (m, 1H). ^{13}C NMR (126 MHz, CD_3OD) δ ppm 42.3, 53.4, 112.0, 115.6, 116.8, 119.9, 123.4, 124.3, 126.7, 128.2, 128.8, 132.3, 133.8, 136.2, 138.5, 148.8. Monoisotopic Mass: 381.15, $[M+H]^+$ 382.2. Elemental analysis calculated for $C_{21}H_{23}N_3O_2S\bullet 2HCl\bullet H_2O$ C: 53.39 %, H: 5.76 %, N: 8.89 %; found C: 53.22 %, H: 5.96 %, N: 9.10 %.

5.1.2.4. *1-(3-(1-(Phenylsulfonyl)-1H-pyrrol-2-yl)phenyl)piperazine (**22**)*.

Following general procedure 1, 3, 4. **Boc-derivative:** yellow oil, 0.175 g (yield 49 %) after flash chromatography purification over silica gel (EtOAc 0−30 % in Hex); UPLC/MS purity 100 %, t_R = 4.37, $C_{25}H_{29}N_3O_4S$, MW 467.58, Monoisotopic Mass 467.19, $[M+H]^+$ 468.2. **Dihydrochloride hydrate**: white solid, 0.121 g (yield 80 %), UPLC/MS purity 100 %, t_R = 2.52, MW 458.40. ^{1}H NMR (400 MHz, CD_3OD) δ ppm 3.41–3.48 (m, 4H), 3.49–3.56 (m, 4H), 6.15 (dd, J = 3.3, 1.7 Hz, 1H), 6.27 (t, J = 3.3 Hz, 1H), 6.76–6.83 (m, 1H), 7.08 (s, 1H), 7.19–7.26 (m, 4H), 7.30 (t, J = 7.2 Hz, 2H), 7.39 (dd, J = 3.4, 1.7 Hz, 1H), 7.46–7.52 (m, 1H). ^{13}C NMR (101 MHz, CD_3OD) δ ppm 42.6, 112.3, 116.2, 118.1, 121.0, 124.6, 126.3, 126.6, 128.6, 128.9, 132.8, 133.9, 135.4, 138.3, 146.2. Monoisotopic Mass: 367.14, $[M+H]^+$ 368.1. Elemental analysis calculated for $C_{20}H_{21}N_3O_2S\bullet 2HCl\bullet H_2O$ C: 52.40 %, H: 5.50 %, N: 9.17 %; found C: 52.41 %, H: 5.97 %, N: 9.18 %.

5.1.2.5. *1-(3-(1-((3-Fluorophenyl)sulfonyl)-1H-pyrrol-2-yl)phenyl)piperazine (**23**)*.

Following general procedure 1, 3, 4. **Boc-derivative:** yellow oil, 0.105 g (yield 47 %) after flash chromatography purification over silica gel (EtOAc 0−20 % in Hex); UPLC/MS purity 99 %, t_R = 9.08, $C_{25}H_{28}FN_3O_4S$, MW 485.57, Monoisotopic Mass 485.18, $[M+H]^+$ 486.2. **Dihydrochloride hydrate**: creamy solid, 0.057 g (yield 62 %), UPLC/MS purity 100 %, t_R = 5.04, MW 476.39. ^{1}H NMR (500 MHz, CD_3OD) δ ppm 3.38–3.43 (m, 4H), 3.44–3.48 (m, 4H), 6.22 (dd, J = 3.2, 1.7 Hz, 1H), 6.36 (t, J = 3.4 Hz, 1H), 6.72–6.77 (m, 1H), 6.94–6.99 (m, 2H), 7.13 (ddd, J = 8.3, 2.6, 0.9 Hz, 1H), 7.16–7.20 (m, 1H), 7.24 (t, J = 8.0 Hz, 1H), 7.34 (tdd, J = 8.5, 8.5, 2.6, 0.9 Hz, 1H), 7.40–7.45 (m, 1H), 7.46 (dd, J = 3.3, 1.6 Hz, 1H). ^{13}C NMR (126 MHz, CD_3OD) δ ppm 43.2, 112.6, 113.9 (d, J = 26.0 Hz), 116.1, 117.4, 120.3, 121.0 (d, J = 23.0

Hz), 122.8 (d, J = 3.6 Hz), 124.3, 124.4, 128.4, 131.2 (d, J = 7.8 Hz), 132.2, 136.1, 140.1 (d, J = 6.6 Hz), 148.5, 161.9 (d, J = 250.5 Hz). Monoisotopic Mass: 385.13, $[M+H]^+$ 386.1. Elemental analysis calculated for $C_{20}H_{20}FN_3O_2S\bullet 2HCl\bullet H_2O$ C: 50.43 %, H: 5.08 %, N: 8.82 %; found C: 50.95 %, H: 5.38 %, N: 9.01 %.

*5.1.2.6. 1-(3-(1-((3-Chlorophenyl)sulfonyl)-1H-pyrrol-2-yl)phenyl)piperazine (**24**).* Following general procedure 1, 3, 4. **Boc-derivative:** colorless oil, 0.269 g (yield 54 %) after flash chromatography purification over silica gel (EtOAc 0−20 % in Hex); UPLC/MS purity 97 %, t_R = 9.45, $C_{25}H_{28}ClN_3O_4S$, MW 502.03, Monoisotopic Mass 501.15, $[M+H]^+$ 502.2. **Dihydrochloride hydrate**: creamy solid, 0.126 g (yield 54 %), UPLC/MS purity 100 %, t_R = 5.33, MW 492.84. ^{1}H NMR (400 MHz, CD_3OD) δ ppm 3.29−3.37 (m, 4H), 3.43−3.47 (m, 4H), 6.25 (dd, J = 3.3, 1.6 Hz, 1H), 6.41 (t, J = 3.3 Hz, 1H), 6.71 (d, J = 7.6 Hz, 1H), 6.87−6.90 (m, 1H), 7.10 (dd, J = 8.0, 2.2 Hz, 1H), 7.19 (t, J = 2.0 Hz, 1H), 7.26 (t, J = 7.6 Hz, 1H), 7.33−7.37 (m, 1H), 7.44 (t, J = 7.9 Hz, 1H), 7.49 (dd, J = 3.4, 1.7 Hz, 1H), 7.63 (ddd, J = 8.0, 2.1, 1.1 Hz, 1H). ^{13}C NMR (101 MHz, CD_3OD) δ ppm 43.4, 46.5, 112.5, 115.9, 117.0, 119.7, 123.4, 124.1, 125.0, 126.8, 128.3, 130.6, 131.9, 133.9, 134.5, 136.2, 139.7, 149.4. Monoisotopic Mass: 401.10, $[M+H]^+$ 402.1. Elemental analysis calculated for $C_{20}H_{20}ClN_3O_2S\bullet 2HCl\bullet H_2O$ C: 48.74 %, H: 4.91 %, N: 8.53 %; found C: 48.98 %, H: 5.33 %, N: 8.61 %.

*5.1.2.7. N-(3-((2-Phenyl-1H-pyrrol-1-yl)sulfonyl)phenyl)piperidin-4-amine (**25**).* Following general procedure 1, 4, 5. **Boc-derivative:** yellow oil, 0.068 g (yield 71 %) after chromatographic purification over silica gel with EtOAc/Hex (3/7, *v/v*); UPLC/MS purity 98 %, t_R = 4.40, $C_{26}H_{31}N_3O_4S$, MW 481.61, Monoisotopic Mass 481.20, $[M+H]^+$ 482.2. **Hydrochloride salt**: creamy solid, 0.044 g (yield 75 %); UPLC/MS purity 100 %, t_R = 5.16, MW 417.95. ^{1}H NMR (400 MHz, CD_3OD) δ ppm 1.76−2.03 (m, 2H), 2.08−2.32 (m, 2H), 3.06−3.23 (m, 2H), 3.42−3.58 (m, 3H), 6.21 (dd, J = 3.3, 1.7 Hz, 1H), 6.39 (t, J = 3.3 Hz, 1H), 6.74−6.78 (m, 2H), 7.04 (dd, J = 8.2, 1.4 Hz, 1H), 7.20−7.26 (m, 3H), 7.29−7.41 (m, 3H), 7.49 (dd, J = 3.4, 1.7 Hz, 1H). ^{13}C NMR (101 MHz, CD_3OD) δ ppm 28.6, 29.5, 44.1, 44.4, 67.5, 113.6, 113.9, 117.8, 118.9, 122.1, 126.3, 129.1, 129.8, 131.8, 132.6, 133.6, 138.2, 141.5, 146.9. Monoisotopic Mass: 381.15, $[M+H]^+$ 382.2. Elemental analysis calculated for $C_{21}H_{23}N_3O_2S\bullet HCl$ C: 60.35 %, H: 5.79 %, N: 10.05 %; found C: 59.89 %, H: 5.45 %, N: 9.98 %.

*5.1.2.8. (R)-N-(3-((2-Phenyl-1H-pyrrol-1-yl)sulfonyl)phenyl)pyrrolidin-3-amine (**26**).* Following general procedure 1, 4, 5. **Boc-derivative:** yellow oil, 0.111 g (yield 72 %) after chromatographic purification over silica gel with EtOAc/Hex (3/7 *v/v*); UPLC/MS purity 100 %, t_R = 9.01, $C_{25}H_{29}N_3O_4S$, MW 467.58, Monoisotopic Mass 467.19, $[M+H]^+$ 468.2. **Dihydrochloride salt**: creamy solid, 0.058 (yield 60 %); UPLC/MS purity 100 %, t_R = 5.08, MW 440.38. ^{1}H NMR (400 MHz, CD_3OD) δ ppm 1.94−2.06 (m, 1H), 2.25−2.37 (m, 1H), 3.11 (dd, J = 12.0, 3.4 Hz, 1H), 3.37−3.52 (m, 3H), 3.98−4.05 (m, 1H), 6.20 (dd, J = 3.2, 1.7 Hz, 1H), 6.38 (t, J = 3.3 Hz, 1H), 6.55 (t, J = 1.9 Hz, 1H), 6.67 (dd, J = 7.8, 0.8 Hz, 1H), 6.86 (dd, J = 8.2, 1.9 Hz, 1H), 7.16 (t, J = 8.0 Hz, 1H), 7.20−7.25 (m, 2H), 7.29−7.35 (m, 2H), 7.35−7.40 (m, 1H), 7.48 (dd, J = 3.3, 1.7 Hz, 1H). ^{13}C NMR (101 MHz, CD_3OD) δ ppm 30.2, 44.0, 49.9, 51.7, 109.3, 111.8, 115.1, 115.6, 118.1, 124.2, 127.1, 127.8, 129.5, 130.6, 131.6, 136.2, 139.4, 147.5. Monoisotopic Mass: 367.14, $[M+H]^+$ 368.1. Elemental analysis calculated for $C_{20}H_{21}N_3O_2S\bullet 2HCl$ C: 54.55 %, H: 5.26 %, N: 9.54 %; found C: 54.61 %, H: 5.04 %, N: 9.85 %.

*5.1.2.9. (S)–N-(3-((2-Phenyl-1H-pyrrol-1-yl)sulfonyl)phenyl)pyrrolidin-3-amine (**27**).* Following general procedure 1, 4, 5. **Boc-derivative:** yellow oil, 0.102 g (yield 66 %) after chromatographic purification over silica gel with EtOAc/Hex (3/7 *v/v*); UPLC/MS purity 100 %, t_R = 9.02, $C_{25}H_{29}N_3O_4S$, MW 467.58, Monoisotopic Mass 467.19, $[M+H]^+$ 468.2. **Dihydrochloride salt**: creamy solid, 0.054 (yield 61 %); UPLC/MS purity 100 %, t_R = 5.13, MW 440.38. ^{1}H NMR (400 MHz, CD_3OD) δ ppm 1.94−2.06 (m, 1H), 2.25−2.37 (m, 1H), 3.11 (dd, J = 12.1, 3.3 Hz, 1H), 3.37−3.50 (m, 3H), 3.97−4.06 (m, 1H), 6.20 (dd, J = 3.2, 1.7 Hz, 1H), 6.38 (t, J = 3.3 Hz, 1H), 6.55 (t, J = 1.9 Hz, 1H), 6.67 (d, J = 7.8 Hz, 1H), 6.86 (dd, J = 8.2, 2.0 Hz, 1H), 7.16 (t, J = 8.0 Hz, 1H), 7.20−7.25 (m, 2H), 7.28−7.35 (m, 2H), 7.35−7.40 (m, 1H), 7.48 (dd, J = 3.3, 1.7 Hz, 1H). ^{13}C NMR (101 MHz, CD_3OD) δ ppm 30.2, 44.0, 49.9. 51.7, 109.3, 111.8, 115.1, 115.6, 118.1, 124.2, 127.1, 127.8, 129.5, 130.6, 131.6, 136.2, 139.4, 147.5. Monoisotopic Mass: 367.14, $[M+H]^+$ 368.1. Elemental analysis calculated for $C_{20}H_{21}N_3O_2S\bullet 2HCl$ C: 54.55 %, H: 5.26 %, N: 9.54 %; found C: 54.76 %, H: 5.47 %, N: 9.23 %.

*5.1.2.10. 1-(3-((2-Phenyl-1H-pyrrol-1-yl)sulfonyl)phenyl)piperazine (**28**).* Following general procedure 1, 4, 6. **Free base:** yellow oil, 0.140 g (yield 57 %) after chromatographic purification over silica gel with MeOH/NH_3 (9/0.05 *v/v*) and DCM/MeOH (9/1.5 *v/v*); UPLC/MS purity 98 %, t_R = 5.04, $C_{20}H_{21}N_3O_2S$, MW 367.47, Monoisotopic Mass 367.14, $[M+H]^+$ 368.1. **Hydrochloride hydrate**: Creamy solid, 0.081 g (yield 53 %); UPLC/MS purity 100 %, t_R = 5.06, MW 421.94. ^{1}H NMR (600 MHz, CD_3OD) δ ppm 3.24−3.27 (m, 4H), 3.30−3.32 (m, 4H), 6.16 (dd, J = 3.3, 1.8 Hz, 1H), 6.33 (t, J = 3.4 Hz, 1H), 6.75 (t, J = 2.2 Hz, 1H), 6.89−6.92 (m, 1H), 7.17−7.21 (m, 3H), 7.27−7.31 (m, 3H), 7.34−7.37 (m, 1H), 7.45 (dd, J = 3.4, 1.7 Hz, 1H). ^{13}C NMR (151 MHz, CD_3OD) δ ppm 43.1, 45.3, 111.9, 113.6, 115.7, 118.2, 121.3, 124.1, 127.1, 127.9, 129.8, 130.7, 131.6, 136.1, 139.3, 150.1. Monoisotopic Mass: 367.14, $[M+H]^+$ 368.1. Elemental analysis calculated for $C_{20}H_{21}N_3O_2S\bullet HCl\bullet H_2O$ C: 56.93 %, H: 5.73 %, N: 9.96 %; found C: 56.89 %, H: 5.74 %, N: 10.14 %.

*5.1.2.11. 1-(3-((2-(2-Fluorophenyl)-1H-pyrrol-1-yl)sulfonyl)phenyl) piperazine (**29**).* Following general procedure 1, 4, 6. **Free base**: yellow oil, 0.184 g (yield 32 %) after chromatographic purification over silica gel with MeOH/NH_3 (9/0.05 *v/v*) and DCM/MeOH (9/1 *v/v*); UPLC/MS purity 100 %, t_R = 5.81, $C_{20}H_{20}FN_3O_2S$, MW 385.46, Monoisotopic Mass 385.13, $[M+H]^+$ 386.1. **Hydrochloride hydrate**: Creamy solid, 0.129 g (yield 64 %); UPLC/MS purity 100 %, t_R = 5.79, MW 439.93. ^{1}H NMR (500 MHz, CD_3OD) δ ppm 3.32−3.35 (m, 8H), 6.21 (dd, J = 3.4, 1.7 Hz, 1H), 6.37 (t, J = 3.3 Hz, 1H), 6.87 (t, J = 2.3 Hz, 1H), 6.93−6.97 (m, 1H), 7.03−7.08 (m, 2H), 7.12 (td, J = 7.6, 1.2 Hz, 1H), 7.24 (ddd, J = 8.3, 2.6, 0.9 Hz, 1H), 7.33 (t, J = 8.3 Hz, 1H), 7.42 (dddd, J = 8.3, 7.4, 5.2, 2.0 Hz, 1H), 7.48 (dd, J = 3.2, 1.7 Hz, 1H). ^{13}C NMR (126 MHz, CD_3OD) δ ppm 43.2, 45.5, 112.1, 113.5, 114.9 (d, J = 23.5 Hz), 116.8, 118.4, 119.7 (d, J = 15.7 Hz), 121.6, 123.0 (d, J = 4.2 Hz), 124.1, 128.5, 130.0, 130.8 (d, J = 8.5 Hz), 133.2 (d, J = 1.8 Hz), 139.5, 150.4, 161.1 (d, J = 248.1 Hz). Monoisotopic Mass: 385.13, [M+H]+ 386.3. Elemental analysis calculated for $C_{20}H_{20}FN_3O_2S\bullet HCl\bullet H_2O$ C: 54.60 %, H: 5.27 %, N: 9.55 %; found C: 54.30 %, H: 5.61 %, N: 9.22 %.

*5.1.2.12. 1-(3-((2-(3-fluorophenyl)-1H-pyrrol-1-yl)sulfonyl)phenyl)piperazine (**30**).* Following general procedure 1, 4, 6. **Free base:** Yellow oil, 0.220 g (yield 48 %) after chromatographic purification over silica gel with MeOH/NH_3 (9/0.05 *v/v*) and DCM/MeOH (9/1 *v/v*); UPLC/MS purity 100 %, t_R = 5.24, $C_{20}H_{20}FN_3O_2S$, MW 385.46, Monoisotopic Mass 385.13, $[M+H]^+$ 386.1. **Hydrochloride hydrate**: Creamy solid, 0.138 g (yield 57 %); UPLC/MS purity 100 %, t_R = 5.23, MW 439.93. ^{1}H NMR (400 MHz, CD_3OD) δ ppm 3.27−3.40 (m, 8H), 6.26 (dd, J = 3.0, 1.5 Hz, 1H), 6.39 (t, J = 3.3 Hz, 1H), 6.86 (s, 1H), 6.91−6.99 (m, 2H), 7.05 (d, J = 7.6 Hz, 1H), 7.16 (td, J = 8.5, 2.1 Hz, 1H), 7.26 (dd, J = 8.3, 1.8 Hz, 1H), 7.31−7.40 (m, 2H), 7.52 (dd, J = 3.1, 1.5 Hz, 1H). ^{13}C NMR (101 MHz, CD_3OD) δ ppm 43.1, 45.3, 112.1, 113.5, 114.7 (d, J = 21.4 Hz), 116.4, 117.3 (d, J = 22.2 Hz), 118.1, 121.4, 124.7, 126.6 (d, J = 2.2 Hz), 128.9 (d, J = 8.4 Hz), 129.9, 133.7 (d, J = 8.4 Hz), 134.6, 139.2, 150.2, 161.8 (d, J = 244.9 Hz). Monoisotopic Mass: 385.13, $[M+H]^+$ 386.1. Elemental analysis calculated for $C_{20}H_{20}FN_3O_2S\bullet HCl\bullet H_2O$ C: 54.60 %, H: 5.27 %, N: 9.55 %; found C: 54.67 %, H: 5.57 %, N: 9.92 %.

*5.1.2.13. 1-(3-((2-(4-Fluorophenyl)-1H-pyrrol-1-yl)sulfonyl)phenyl) piperazine (**31**).* Following general procedure 1, 4, 6. **Free base:** Yellow oil, 0.170 g (yield 30 %) after chromatographic purification over silica gel with MeOH/NH_3 (9/0.05 *v/v*) and DCM/MeOH (9/1.5 *v/v*); UPLC/MS purity 100 %, t_R = 5.93, $C_{20}H_{20}FN_3O_2S$, MW 385.46, Monoisotopic Mass 385.13, $[M+H]^+$ 386.1. **Dihydrochloride hydrate**: Creamy solid, 0.155 g (yield 83 %); UPLC/MS purity 100 %, t_R = 5.95, MW 476.39, ^{1}H NMR (500 MHz, CD_3OD) δ ppm 3.30−3.34 (m, 8H), 6.16 (dd, J = 3.2, 1.7 Hz, 1H), 6.33 (t, J = 3.3 Hz, 1H), 6.80 (t, J = 2.3 Hz, 1H), 6.87−6.90 (m, 1H), 7.01−7.06 (m, 2H), 7.15−7.19 (m, 2H), 7.21 (ddd, J = 8.4, 2.5, 0.9 Hz, 1H), 7.30 (t, J = 8.3 Hz, 1H), 7.45 (dd, J = 3.4, 1.7 Hz, 1H). ^{13}C NMR (126 MHz, CD_3OD) δ ppm 43.2, 45.4, 111.9, 113.7, 114.0 (d, J = 22.3 Hz), 115.9, 118.2, 121.4, 124.2, 127.8 (d, J = 3.6 Hz), 130.0, 132.8 (d, J = 7.9 Hz), 134.8, 139.3, 150.2, 162.9 (d, J = 245.7 Hz). ^{19}F NMR (471 MHz, $CDCl_3$) δ ppm −116.16 (tt, J = 8.8, 5.4 Hz). Monoisotopic Mass: 385.13, $[M+H]^+$ 386.1. Elemental analysis calculated for $C_{20}H_{20}FN_3O_2S\bullet 2HCl\bullet H_2O$ C: 50.43 %, H: 5.08 %, N: 8.82 %; found C: 50.76 %, H: 5.32 %, N: 8.85 %.

*5.1.2.14. 1-(3-((2-(3-Chlorophenyl)-1H-pyrrol-1-yl)sulfonyl)phenyl) piperazine (**32**).* Following general procedure 1, 4, 6. **Free base**: Yellow oil, 0.210 g (yield 44 %) after chromatographic purification over silica gel with MeOH/NH_3 (9/0.05 *v/v*) and DCM/MeOH (9/1.5 *v/v*); UPLC/MS purity 98 %, t_R = 5.57, $C_{20}H_{20}ClN_3O_2S$, MW 401.91, Monoisotopic Mass 401.10, $[M+H]^+$ 402.1. **Hydrochloride hydrate**: Creamy solid, 0.102 g (yield 46 %); UPLC/MS purity 100 %, t_R = 5.55, MW 456.38. ^{1}H NMR (500 MHz, CD_3OD) δ ppm 3.30−3.35 (m, 8H), 6.22 (dd, J = 2.9, 1.7 Hz, 1H), 6.35 (t, J = 3.4 Hz, 1H), 6.80 (t, J = 2.3 Hz, 1H), 6.91−6.95 (m, 1H), 7.08 (t, J = 1.7 Hz, 1H), 7.15−7.19 (m, 1H), 7.21−7.24 (m, 1H), 7.29−7.34 (m, 2H), 7.36−7.39 (m, 1H), 7.48 (dd, J = 3.4, 1.7 Hz, 1H). ^{13}C NMR (126 MHz, $CDCl_3$) δ ppm 43.2, 45.4, 112.1, 113.6, 116.4, 118.2, 121.5, 124.7, 128.0, 128.8, 129.3, 130.0, 130.3, 132.9, 133.5, 134.4, 139.2, 150.3. Monoisotopic Mass: 401.10, $[M+H]^+$ 402.1. Elemental analysis calculated for $C_{20}H_{20}ClN_3O_2S\bullet HCl\bullet H_2O$ C: 52.64 %, H: 5.08 %, N: 9.21 %; found C: 52.89 %, H: 4.84 %, N: 9.44 %.

*5.1.2.15. 1-(3-((2-(3-Methoxyphenyl)-1H-pyrrol-1-yl)sulfonyl)phenyl) piperazine (**33**).* Following general procedure 1, 4, 6. **Free base**: Yellow oil, 0.160 g (yield 26 %) after chromatographic purification over silica gel with MeOH/NH_3 (9/0.05 *v/v*) and DCM/MeOH (9/1.5 *v/v*); UPLC/MS purity 98 %, t_R = 5.90, $C_{21}H_{23}N_3O_3S$, MW 397.49, Monoisotopic Mass 397.15, $[M+H]^+$ 398.2. **Dihydrochloride hydrate**: Creamy solid, 0.148 g (yield 85 %); UPLC/MS purity 100 %, t_R = 5.92, MW 488.42. ^{1}H NMR (500 MHz, CD_3OD) δ ppm 3.25−3.33 (m, 8H), 3.73 (s, 3H), 6.16 (dd, J = 3.3, 1.9 Hz, 1H), 6.3 (t, J = 3.3 Hz, 1H), 6.69 (dd, J = 2.6, 1.4 Hz, 1H), 6.75−6.78 (m, 2H), 6.93 (tdd, J = 8.2, 8.2, 2.2, 0.9 Hz, 2H), 7.18−7.22 (m, 2H), 7.30 (t, J = 8.0 Hz, 1H), 7.45 (dd, J = 3.3, 1.9 Hz, 1H). ^{13}C NMR (126 MHz, $CDCl_3$) δ ppm 14.1, 43.2, 45.3, 54.5, 65.6, 111.9, 113.8, 114.0, 115.7, 116.0, 118.3, 121.3, 123.2, 124.1, 128.2, 129.9, 132.8, 135.9, 139.3, 150.1, 158.8. Monoisotopic Mass: 397.15, $[M+H]^+$ 398.2. Elemental analysis calculated for $C_{21}H_{23}N_3O_2S\bullet 2HCl\bullet H_2O$ C: 51.64 %, H: 5.57 %, N: 8.60 %; found C: 51.57 %, H: 5.41 %, N: 8.47 %.

5.2. In vitro pharmacological evaluation

5.2.1. 5-HT$_6$R affinity and selectivity evaluation. Radioligand binding assays

The experiments were carried out according to the previously published protocols [25,40]. HEK293 cell line stably expressing human 5-HT_{1A}, 5-HT_6, 5-HT_{7b} and D_{2L} receptors (prepared with the use of Lipofectamine 2000) or CHO–K1 cells transfected with plasmid containing the sequence coding for the human serotonin 5-HT_{2A} receptor (PerkinElmer) were maintained at 37 °C in a humidified atmosphere containing 5 % CO_2 and grown in Dulbecco's Modified Eagle's Medium containing 10 % dialyzed fetal bovine serum and 500 μg/ml G418 sulfate. For membrane preparation, cells were cultured in 150 cm^2 flasks, grown to 90 % confluence, washed twice with pre-warmed to 37 °C phosphate buffered saline (PBS) and centrifuged (200×*g*) in PBS containing 0.1 mM EDTA and 1 mM dithiothreitol. The cell pellets were preserved at −80 °C until the commencement of membrane isolation The pellets were first thawed and then homogenized in 10 vol of assay buffer using an Ultra Turrax tissue homogenizer and centrifuged twice at 35,000×*g* for 15 min at 4 °C, with incubation for 15 min at 37 °C between the centrifugations. The composition of the assay buffers was determined through experimental processes designed to maximize the signal window as previously reported [25,40]. The experimental assays were then conducted in a uniform volume of 200 μL in 96-well plates for 1 h at 37 °C, except 5-HT_{1A} receptor and 5-HT_{2A} receptor which were incubated at rt and 27 °C, respectively. The equilibrium process was halted through swift filtration using GF/C UniFilter plates (PerkinElmer, USA) with a 96-well cell harvester and radioactivity retained on the filters was quantified on a Microbeta plate reader (PerkinElmer, USA). For displacement studies the assay samples contained as radioligands (PerkinElmer, USA): 2.5 nM [^{3}H]-8-OH-DPAT (135.2 Ci/mmol) for 5-HT_{1A} receptor; 1 nM [^{3}H]-ketanserin (53.4 Ci/mmol) for 5-HT_{2A} receptor; 2 nM [^{3}H]-LSD (83.6 Ci/mmol) for 5-HT_6 receptor; 0.8 nM [^{3}H]-5-CT (39.2 Ci/mmol) for 5-HT_7 receptor or 2.5 nM [^{3}H]-raclopride (76.0 Ci/mmol) for D_{2L} receptor. Non-specific binding was defined in the presence of 10 μM of 5-HT in 5-HT_{1A} receptor and 5-HT_7 receptor binding experiments, whereas 20 μM of mianserin, 10 μM of methiothepine or 10 μM of haloperidol were used in 5-HT_{2A} receptor, 5-HT_6R and D_{2L} receptor assays, respectively. Each compound was tested across 7 concentrations ranging from 10^{-10} to10^{-4} M. The inhibition constants (K_i) were calculated from the Cheng-Prusoff equation [41].

5.2.2. Functional profiling at 5-HT$_6$R-operated Gs signaling

5.2.2.1. Determination of cAMP production in 1321N1 cells. The effect of compounds **22**, **25**, **28**, **and 30** to inhibit cAMP production induced by a 5-HT_6R agonist (5-CT, 1000 nM) was evaluated using frozen recombinant 1321N1 cells expressing the human 5-HT_6R (PerkinElmer). The compounds were tested across 8 concentrations ranging from 10^{-11} to 10^{-4} M. The quantification was carried out using the LANCE cAMP detection kit (PerkinElmer), according to the manufacturer's recommendations. For quantification of cAMP levels, 2000 cells/well (5 μL) were incubated with mixture of compounds (5 μL) for 30 min at rt in 384-well white opaque microtiter plate. The process was halted and the cells were lysed by adding 10 μL of the working solution (5 μL Eu-cAMP and 5 μL ULight-anti-cAMP) for 1 h at rt. Time-resolved fluorescence resonance energy transfer (TR-FRET) was detected by an Infinite M1000 Pro (Tecan) using instrument settings from LANCE cAMP detection kit manual. The K_b value for each inhibitor was determined using modified Cheng–Prusoff equation as reported in Ref. [42], specific for the analysis of functional inhibition curves: $K_b = IC_{50}/(1+A/EC_{50})$ where A represents the agonist concentration, IC_{50} - the concentration of antagonist producing a 50 % reduction in the response to agonist, and EC_{50} - the agonist concentration which causes a half of the maximal response.

5.2.2.2. Determination of cAMP production in NG108-15 cells. NG108-15 cells were cultured in Dulbecco's modified Eagle's medium (DMEM), 10 % decomplemented fetal bovine serum, 2 % hypoxanthine/aminopterin/thymidine (Life Technologies) and antibiotics, at 37 °C under 5 % CO_2. Measurement of cAMP production was performed in cells overexpressing the 5-HT_6R using a bioluminescence resonance energy transfer (BRET) probe, CAMYEL (cAMP sensor using YFP-Epac-RLuc) [31]. Co-transfection of 5-HT_6R (1ug DNA/1 million cells) and CAMYEL (4ug DNA/1 million cells) was performed in suspension using lipofectamine 2000, following the protocol recommended by the supplier. The cells were then seeded in a white 96-well plate (Greiner) at a

density of 50,000 cells per well in DMEM 2 % decomplemented fetal bovine serum, 2 % hypoxanthine/aminopterin/thymidine (Life Technologies) and antibiotics. 48 h after transfection, cells were treated with the tested compounds or vehicle at concentrations ranging from 10 nM to 10 μM. Coelanterazine 1H (Molecular Probes) was added at a final concentration of 5 μM. The BRET signal was measured using the Mithras LB 940 plate reader (Berthold Technologies). This decrease in the CAMYEL BRET signal was thus used as an index of 5-HT_6R constitutive activity at Gs signaling.

5.2.3. Functional profiling at 5-HT_6R-operated Cdk5 signaling

NG108-15 cells were transfected with plasmids encoding either cytosolic YFP or a YFP-tagged 5-HT_6R in suspension using Lipofectamine 2000 (Life Technologies) and plated on glass coverslips. Six hours after transfection, cells were treated with either DMSO (control), compound **28**, **30,** PZ-1388 or intepirdine (10^{-6} M) for 48 h. Cells were fixed in 4 % paraformaldehyde (PFA) for 10 min. PFA fluorescence was quenched by incubating the cells in PBS containing 0.1 M glycine for 15 min, prior to mounting in Dako reagent (Dako). Cells were imaged using an AxioImagerZ1 microscope equipped with epifluorescence (Zeiss), using a 20 × objective for cultured cells, and neurite length was assessed using the Neuron J plugin of the ImageJ software (NIH).

5.3. Molecular modeling

5.3.1. Structures of the receptors

The conformation of the 5-HT_6R receptor bound to the serotonin agonist was analyzed using its structure (PDB ID: 7XTB) [43] obtained from the Protein Data Bank [44]. The sequence-based generic GPCR residue numbering scheme was used to unify the amino acid notation [33].

5.3.2. Conformational Adjustment through docking

The receptor's conformation was adapted for the target compounds using the Induced Fit Docking (IFD) approach from the Schrödinger software suite. The 5-HT_6R structure underwent preparation that involved bond order assignment, setting correct amino acid ionization states, and resolving steric conflicts, employing the Protein Preparation Wizard in the Schrödinger Suite. Ligand structures were processed using LigPrep v3.6, and their ionization states at pH 7.4 ± 1.0 were estimated with Epik v3.4. A 10 Å grid box was set around the crystallized ligand, and comprehensive searching was executed. Ligand-receptor complexes, identified through IFD, were then utilized in subsequent molecular dynamics studies.

5.3.3. Molecular dynamics simulations

Molecular dynamics simulations, extending over 100 ns, were conducted using Desmond software from Schrödinger [45]. The ligand-receptor complexes were embedded in a POPC membrane bilayer at 309.5 K, its positioning determined via the PPM web server (accessed March 10, 2023) [46]. The system was hydrated with water molecules, represented by the TIP4P model, and the OPLS3 force field applied to all atomic structures. To replicate cellular ionic conditions, 0.15 M NaCl was included. Output trajectories underwent hierarchical clustering into five categories based on the backbones, employing Schrödinger's trajectory analysis tool.

5.3.4. Observation of receptor structural alterations

Alterations in the 5-HT_6R helices during the molecular dynamics of the receptor with different agonist and antagonist pairs (**22** *vs* PZ-1388, **28** *vs* PZ-1388, **22** *vs* CPPQ, **28** *vs* CPPQ) were observed. Spatial coordinates (x,y,z) of specific amino acids were reduced to single centroid points. This method enabled the tracking of amino acid movement through the trajectory of these points. Variations in receptor conformation were quantified by measuring the Euclidean distances between centroids of identical amino acids, referred to as Δd. This centroid-based method of tracking amino acid movements has been well-established and effectively employed in previous studies, providing rational and reliable results. It offers a precise and systematic approach to quantifying conformational changes in receptor structures, thereby facilitating a deeper understanding of ligand-receptor interactions [20,35].

5.4. Preliminary in vitro ADME/Tox assessment

5.4.1. In vitro metabolic stability study

The metabolic stability of compounds **22**, **25**, **28**, **30**, and **33** was assessed following previously reported procedures [21,25,47]. Solutions of the tested compounds (final concentration = 10 μM) were pre-incubated in phosphate buffer (pH = 7.4) containing rat liver microsomes (RLMs, microsomes from rat male liver, pooled, 0.5 mg/mL, Merck/Millipore Sigma, Darmstadt, Germany) for 10 min at 37 °C. The reaction was initiated by adding the NADPH-regenerating system (NADP+, glucose-6-phosphate, and glucose-6-phosphate dehydrogenase in 100 mM potassium buffer, pH 7.4; all from Sigma Aldrich) and incubated for 0, 30, and 60 min at 37 °C. In control samples, the NADPH-regenerating system was replaced with a potassium buffer. The reaction was quenched by the addition of an ice-cold methanolic solution of the internal standard (pentoxifylline, 100 nM). Samples were then centrifuged, and the supernatants were analyzed by UPLC/MS. All experiments were conducted in duplicate. The half-life time ($t_{1/2}$) was determined from the slope of the line on Ln (% remaining of parent compounds) *vs.* time plots. Cl_{int} was calculated from the equation: Cl_{int} = [volume of incubation (μL)/amount of protein (mg) × 0.693]/$t_{1/2}$. The assay performance was confirmed using imipramine, an extensively metabolized drug, as a references.

5.4.2. Off-target affinity assessment

The affinity of compound **30** at the H_3 receptor, D_3 receptor, σ_1 receptor, *h*ERG channel, and CYP3A4 were evaluated in Eurofins. The results were expressed as the % inhibition at 1 μM (for H_3 receptor, D_3 receptor, σ_1 receptor, *h*ERG) and 10 μM (for CYP3A4) according to experimental protocols described online at https://www.eurofins.com/.

5.5. Cytoprotection studies

5.5.1. Cell culture

Rat pheochromocytoma PC12 Adh (CRL1721.1), human neuroblastoma SHSY-5Y (CRL-2266), and mouse astrocytes C8-D1A (CRL2541) were cultured in appropriate media recommended by ATCC supplemented with 10 % fetal bovine serum (FBS) and 1 % penicillin/streptomycin solution. Cells were cultured in standard conditions (37 °C, 5 % CO_2, and 95 % humidity) and subcultured when they reached 80 % confluency or above.

Immortalized Human Astrocytes (P10251-IM) were purchased from Innoprot company (Spain) and cultured according to the manufacturer's protocol in Astrocyte Medium supplemented with 5 % FBS, 1 % Astrocyte Medium Growth Supplement, and 1 % penicillin/streptomycin solution. Cells were grown under standard conditions (37 °C, 5 % CO_2, and 95 % humidity) in cell dishes coated with poly-L-lysine. Cells were subcultured when they reached 90 % confluency or above.

5.5.2. Experimental conditions

Cells were preincubated with fresh culture medium without compounds (controls) or with analyzed compounds (0.25 μM) for 3 h. Next, the medium was replaced with fresh medium containing damaging agents (β-amyloid-2.5 μM, rotenone-0.5 μM, and 6OHDA-20μM) for an additional 24 h.

5.5.3. MTT assay

For viability assays, cells were seeded in 96-well plates at a concentration of 1 × 10^4 cells per well and cultured as described in the experimental condition section. A colorimetric MTT assay was used to

evaluate cell viability. Specifically, 10 μL of MTT reagent was added to each well. After 4 h of incubation at 37 °C with 5 % CO_2, the medium was aspirated, and the formed formazan crystals were dissolved with 100 μL of DMSO solution. The optical density (OD) at 570 nm was then determined using a plate reader (Spectra Max iD3, Molecular Devices). Each experiment was repeated at least three times.

5.5.4. CytoTox-Glo assay

The CytoTox-Glo cell membrane integrity test (Promega) was used for cytotoxicity testing following the manufacturer's protocol. Astrocytes were seeded at a density of 2×10^4 cells/well in white 96-well culture plates and incubated for 24 h. The cells were then incubated in the presence of the analyzed compounds for 3 h (0.25 μM), followed by a change of culture medium to fresh medium containing Rot −0.5 μM for the next 24 h. Triton X-100 was used as a positive control. CytoTox-Glo™ reagent was added to each well, and luminescence signals were measured with a microplate reader (Spectra Max ID3, Molecular Devices) (signal 1). Subsequently, lysis solution was added and incubated for 15 min to detect the total signal, and luminescence was measured again (signal 2). The percentage of living cells was calculated by subtracting signal 1 from signal 2. The signal of the control condition was set to 100 %, and the signal of TritonX-100 to 0 % living cells. Cytotoxicity was calculated as 100-A, where A is the viability of the cells in the analyzed sample relative to controls.

5.5.5. Actin cytoskeleton organization

To visualize the actin cytoskeleton, cells were seeded on glass coverslips inserted into 12-well plates at a density of 2×10^4 cells/well and cultivated for 24 h. The cells were cultured as described in the Experimental condition section. Subsequently, the cells were washed with PBS containing Ca^{2+} and Mg^{2+} ions, fixed in 3.7 % paraformaldehyde/PBS at room temperature, and permeabilized with 0.1 % Triton X-100/PBS for 6 min. Next, a phalloidin solution (500 ng/mL, Sigma-Aldrich) in PBS, counterstained with Hoechst 33342, was added for 45 min. The slides were mounted in ProLong™ Glass Antifade Mountant and analyzed using a Leica DMiL LED Fluo microscope equipped with LAS-X Software (40 × objective). Experiments were repeated three times using five randomly selected fields of view, with the same fluorescent time exposure, and in a blind-folded manner.

5.5.6. Statistical analysis

Data normality was checked using Shapiro-Wilk test. Data are expressed as mean ± SD. Statistically significant values were compared using the Brown–Forsythe and Welch's ANOVA tests, along with the post-hoc unpaired *t*-test with Welch's correction. The GraphPad Prism 5 software, and p-values of <0.05 was considered statistically significant.

CRediT authorship contribution statement

Marcin Drop: Writing – review & editing, Writing – original draft, Investigation, Funding acquisition, Conceptualization. **Paulina Koczurkiewicz-Adamczyk:** Writing – original draft, Methodology, Investigation. **Ophélie Bento:** Investigation. **Wojciech Pietruś:** Methodology, Investigation. **Grzegorz Satała:** Methodology, Investigation. **Klaudia Blicharz-Futera:** Investigation. **Vittorio Canale:** Methodology, Investigation. **Katarzyna Grychowska:** Investigation. **Xavier Bantreil:** Methodology. **Elżbieta Pękala:** Supervision. **Rafał Kurczab:** Supervision, Methodology. **Andrzej J. Bojarski:** Supervision. **Severine Chaumont-Dubel:** Writing – review & editing, Supervision, Methodology, Investigation. **Philippe Marin:** Supervision, Methodology, Formal analysis. **Frédéric Lamaty:** Supervision, Methodology, Formal analysis. **Paweł Zajdel:** Writing – review & editing, Writing – original draft, Supervision, Methodology, Funding acquisition, Conceptualization.

Declaration of competing interest

All authors disclose no financial or personal relationships that may be perceived as influencing their work.

Data availability

Data will be made available on request.

Acknowledgments

The studies were funded by the National Science Centre, Poland, grant no 2019/33/N/NZ7/01875. MD was supported by the Foundation for Polish Science (START programme), Jagiellonian Interdisciplinary PhD Programme, French Government Scholarship, and the statutory activity funds of Jagiellonian University Medical College. Some of the experiments were carried out with equipment co-financed by the qLIFE Priority Research Area under the program "Excellence Initiative—Research University" at Jagiellonian University. The MPO values were calculated using *Instant JChem* (ChemAxon). The graphical abstract was created with BioRender.com.

Appendix A. Supplementary data

Supplementary data to this article can be found online at https://doi.org/10.1016/j.ejmech.2024.116615.

References

[1] M. Berger, J.A. Gray, B.L. Roth, The expanded biology of serotonin, Annu. Rev. Med. 60 (2009) 355–366, https://doi.org/10.1146/annurev.med.60.042307.110802.
[2] M. Pourhamzeh, F.G. Moravej, M. Arabi, E. Shahriari, S. Mehrabi, R. Ward, R. Ahadi, M.T. Joghataei, The roles of serotonin in neuropsychiatric disorders, Cell. Mol. Neurobiol. 42 (2022) 1671–1692, https://doi.org/10.1007/s10571-021-01064-9.
[3] N.M. Barnes, G.P. Ahern, C. Becamel, J. Bockaert, M. Camilleri, S. Chaumont-Dubel, S. Claeysen, K.A. Cunningham, K.C. Fone, M. Gershon, G.D. Giovanni, N. M. Goodfellow, A.L. Halberstadt, R.M. Hartley, G. Hassaine, K. Herrick-Davis, R. Hovius, E. Lacivita, E.K. Lambe, M. Leopoldo, F.O. Levy, S.C.R. Lummis, P. Marin, L. Maroteaux, A.C. McCreary, D.L. Nelson, J.F. Neumaier, A. Newman-Tancredi, H. Nury, A. Roberts, B.L. Roth, A. Roumier, G.J. Sanger, M. Teitler, T. Sharp, C.M. Villalón, H. Vogel, S.W. Watts, D. Hoyer, International union of basic and clinical pharmacology. CX. Classification of receptors for 5-hydroxytryptamine; pharmacology and function, Pharmacol. Rev. 73 (2021) 310–520, https://doi.org/10.1124/pr.118.015552.
[4] X. Codony, J.M. Vela, M.J. Ramírez, 5-HT(6) receptor and cognition, Curr. Opin. Pharmacol. 11 (2011) 94–100, https://doi.org/10.1016/j.coph.2011.01.004.
[5] H. Ferrero, M. Solas, P.T. Francis, M.J. Ramirez, Serotonin 5-HT6 receptor antagonists in Alzheimer's disease: therapeutic rationale and current development status, CNS Drugs 31 (2017) 19–32, https://doi.org/10.1007/s40263-016-0399-3.
[6] I.E.M. de Jong, A. Mørk, Antagonism of the 5-HT6 receptor - preclinical rationale for the treatment of Alzheimer's disease, Neuropharmacology 125 (2017) 50–63, https://doi.org/10.1016/j.neuropharm.2017.07.010.
[7] R. Khoury, N. Grysman, J. Gold, K. Patel, G.T. Grossberg, The role of 5 HT6-receptor antagonists in Alzheimer's disease: an update, Expet Opin. Invest. Drugs 27 (2018) 523–533, https://doi.org/10.1080/13543784.2018.1483334.
[8] R. Nirogi, P. Jayarajan, A. Shinde, A.R. Mohammed, V.R. Grandhi, V. Benade, V. K. Goyal, R. Abraham, V. Jasti, J. Cummings, Progress in investigational agents targeting serotonin-6 receptors for the treatment of brain disorders, Biomolecules 13 (2023) 309, https://doi.org/10.3390/biom13020309.
[9] S. Chaumont-Dubel, V. Dupuy, J. Bockaert, C. Bécamel, P. Marin, The 5-HT6 receptor interactome: new insight in receptor signaling and its impact on brain physiology and pathologies, Neuropharmacology 172 (2020) 107839, https://doi.org/10.1016/j.neuropharm.2019.107839.
[10] H.-M. Yun, S. Kim, H.-J. Kim, E. Kostenis, J.I. Kim, J.Y. Seong, J.-H. Baik, H. Rhim, The novel cellular mechanism of human 5-HT6 receptor through an interaction with Fyn, J. Biol. Chem. 282 (2007) 5496–5505, https://doi.org/10.1074/jbc.M606215200.
[11] J. Bockaert, P. Marin, mTOR in brain physiology and pathologies, Physiol. Rev. 95 (2015) 1157–1187, https://doi.org/10.1152/physrev.00038.2014.
[12] P. De Deurwaerdère, R. Bharatiya, A. Chagraoui, G. Di Giovanni, Constitutive activity of 5-HT receptors: factual analysis, Neuropharmacology 168 (2020) 107967, https://doi.org/10.1016/j.neuropharm.2020.107967.
[13] R. Kohen, L.A. Fashingbauer, D.E. Heidmann, C.R. Guthrie, M.W. Hamblin, Cloning of the mouse 5-HT6 serotonin receptor and mutagenesis studies of the third

cytoplasmic loop, Brain Res. Mol. Brain Res. 90 (2001) 110–117, https://doi.org/10.1016/s0169-328x(01)00090-0.
[14] W. Deraredj Nadim, S. Chaumont-Dubel, F. Madouri, L. Cobret, M.-L. De Tauzia, P. Zajdel, H. Bénédetti, P. Marin, S. Morisset-Lopez, Physical interaction between neurofibromin and serotonin 5-HT6 receptor promotes receptor constitutive activity, Proc. Natl. Acad. Sci. U.S.A. 113 (2016) 12310–12315, https://doi.org/10.1073/pnas.1600914113.
[15] F. Duhr, P. Déléris, F. Raynaud, M. Séveno, S. Morisset-Lopez, C. Mannoury la Cour, M.J. Millan, J. Bockaert, P. Marin, S. Chaumont-Dubel, Cdk5 induces constitutive activation of 5-HT6 receptors to promote neurite growth, Nat. Chem. Biol. 10 (2014) 590–597, https://doi.org/10.1038/nchembio.1547.
[16] M. Jacobshagen, M. Niquille, S. Chaumont-Dubel, P. Marin, A. Dayer, The serotonin 6 receptor controls neuronal migration during corticogenesis via a ligand-independent Cdk5-dependent mechanism, Development 141 (2014) 3370–3377, https://doi.org/10.1242/dev.108043.
[17] A.B. Allnutt, A.K. Waters, S. Kesari, V.M. Yenugonda, Physiological and pathological roles of Cdk5: potential directions for therapeutic targeting in neurodegenerative disease, ACS Chem. Neurosci. 11 (2020) 1218–1230, https://doi.org/10.1021/acschemneuro.0c00096.
[18] A.M. Bokare, A.K. Praveenkumar, M. Bhonde, Y. Nayak, R. Pal, R. Goel, 5-HT6 receptor agonist and antagonist against β-amyloid-peptide-induced neurotoxicity in PC-12 cells, Neurochem. Res. 42 (2017) 1571–1579, https://doi.org/10.1007/s11064-017-2217-9.
[19] P. Pyka, W. Haberek, M. Więcek, E. Szymanska, W. Ali, A. Cios, M. Jastrzębska-Więsek, G. Satała, S. Podlewska, S. Di Giacomo, A. Di Sotto, S. Garbo, T. Karcz, C. Lambona, F. Marocco, G. Latacz, S. Sudoł-Tałaj, B. Mordyl, M. Głuch-Lutwin, A. Siwek, K. Czarnota-Łydka, D. Gogola, A. Olejarz-Maciej, N. Wilczyńska-Zawal, E. Honkisz-Orzechowska, M. Starek, M. Dąbrowska, K. Kucwaj-Brysz, R. Fioravanti, M.J. Nasim, M. Hittinger, A. Partyka, A. Wesołowska, C. Battistelli, C. Zwergel, J. Handzlik, First-in-Class selenium-containing potent serotonin receptor 5-HT6 agents with a beneficial neuroprotective profile against Alzheimer's disease, J. Med. Chem. (2024), https://doi.org/10.1021/acs.jmedchem.3c02148.
[20] D. Vanda, V. Canale, S. Chaumont-Dubel, R. Kurczab, G. Satała, P. Koczurkiewicz-Adamczyk, M. Krawczyk, W. Pietruś, K. Blicharz, E. Pękala, A.J. Bojarski, P. Popik, P. Marin, M. Soural, P. Zajdel, Imidazopyridine-based 5-HT6 receptor neutral antagonists: impact of N1-benzyl and N1-phenylsulfonyl fragments on different receptor conformational states, J. Med. Chem. 64 (2021) 1180–1196, https://doi.org/10.1021/acs.jmedchem.0c02009.
[21] V. Canale, W. Trybała, S. Chaumont-Dubel, P. Koczurkiewicz-Adamczyk, G. Satała, O. Bento, K. Blicharz-Futera, X. Bantreil, E. Pękala, A.J. Bojarski, F. Lamaty, P. Marin, P. Zajdel, 1-(Arylsulfonyl-isoindol-2-yl)piperazines as 5-HT6R antagonists: mechanochemical synthesis, in vitro pharmacological properties and glioprotective activity, Biomolecules 13 (2022) 12, https://doi.org/10.3390/biom13010012.
[22] K. Grychowska, S. Chaumont-Dubel, R. Kurczab, P. Koczurkiewicz, C. Deville, M. Krawczyk, W. Pietruś, G. Satała, S. Buda, K. Piska, M. Drop, X. Bantreil, F. Lamaty, E. Pękala, A.J. Bojarski, P. Popik, P. Marin, P. Zajdel, Dual 5-HT6 and D3 receptor antagonists in a group of 1 H-Pyrrolo[3,2- c]quinolines with neuroprotective and procognitive activity, ACS Chem. Neurosci. (2019), https://doi.org/10.1021/acschemneuro.8b00618.
[23] K. Grychowska, U. López-Sánchez, M. Vitalis, G. Canet, G. Satała, A. Olejarz-Maciej, J. Gołębiowska, R. Kurczab, W. Pietruś, M. Kubacka, C. Moreau, M. Walczak, K. Blicharz-Futera, O. Bento, X. Bantreil, G. Subra, A.J. Bojarski, F. Lamaty, C. Becamel, C. Zussy, S. Chaumont-Dubel, P. Popik, H. Nury, P. Marin, L. Givalois, P. Zajdel, Superiority of the triple-acting 5-HT6R/5-HT3R antagonist and MAO-B reversible inhibitor PZ-1922 over 5-HT6R antagonist intepirdine in alleviation of cognitive deficits in rats, J. Med. Chem. 66 (2023) 14928–14947, https://doi.org/10.1021/acs.jmedchem.3c01482.
[24] P. Zajdel, M. Drop, V. Canale, M. Pawłowski, G. Satała, A. Bojarski, G. Subra, J. Martinez, X. Bantreil, F. Lamaty, P.-Y. Martin, C. Courteix, S. Chaumont-Dubel, P. Marin, Arylsulfonamides of 2-arylpyrrole-3-carboxamides for the treatment of cns disorders, WO2020117075A1 (2020). https://patents.google.com/patent/WO2020117075A1/en. (Accessed 14 October 2020).
[25] M. Drop, V. Canale, S. Chaumont-Dubel, R. Kurczab, G. Satała, X. Bantreil, M. Walczak, P. Koczurkiewicz-Adamczyk, G. Latacz, A. Gwizdak, M. Krawczyk, J. Gołębiowska, K. Grychowska, A.J. Bojarski, A. Nikiforuk, G. Subra, J. Martinez, M. Pawłowski, P. Popik, P. Marin, F. Lamaty, P. Zajdel, 2-Phenyl-1H-pyrrole-3-carboxamide as a new scaffold for developing 5-HT6 receptor inverse agonists with cognition-enhancing activity, ACS Chem. Neurosci. 12 (2021) 1228–1240, https://doi.org/10.1021/acschemneuro.1c00061.
[26] P.-Y. Martin, S. Doly, A.M. Hamieh, E. Chapuy, V. Canale, M. Drop, S. Chaumont-Dubel, X. Bantreil, F. Lamaty, A.J. Bojarski, P. Zajdel, A. Eschalier, P. Marin, C. Courteix, mTOR activation by constitutively active serotonin6 receptors as new paradigm in neuropathic pain and its treatment, Prog. Neurobiol. 193 (2020) 101846, https://doi.org/10.1016/j.pneurobio.2020.101846.
[27] B. Benhamú, M. Martín-Fontecha, H. Vázquez-Villa, L. Pardo, M.L. López-Rodríguez, Serotonin 5-HT6 receptor antagonists for the treatment of cognitive deficiency in Alzheimer's disease, J. Med. Chem. 57 (2014) 7160–7181, https://doi.org/10.1021/jm5003952.
[28] V. Canale, K. Grychowska, R. Kurczab, M. Ryng, A.R. Keeri, G. Satała, A. Olejarz-Maciej, P. Koczurkiewicz, M. Drop, K. Blicharz, K. Piska, E. Pękala, P. Janiszewska, M. Krawczyk, M. Walczak, S. Chaumont-Dubel, A.J. Bojarski, P. Marin, P. Popik, P. Zajdel, A dual-acting 5-HT6 receptor inverse agonist/MAO-B inhibitor displays glioprotective and pro-cognitive properties, Eur. J. Med. Chem. 208 (2020) 112765, https://doi.org/10.1016/j.ejmech.2020.112765.
[29] K. Grychowska, G. Satała, T. Kos, A. Partyka, E. Colacino, S. Chaumont-Dubel, X. Bantreil, A. Wesołowska, M. Pawłowski, J. Martinez, P. Marin, G. Subra, A. J. Bojarski, F. Lamaty, P. Popik, P. Zajdel, Novel 1H-Pyrrolo[3,2-c]quinoline based 5-HT6 receptor antagonists with potential application for the treatment of cognitive disorders associated with Alzheimer's disease, ACS Chem. Neurosci. 7 (2016) 972–983, https://doi.org/10.1021/acschemneuro.6b00090.
[30] D. Vanda, M. Soural, V. Canale, S. Chaumont-Dubel, G. Satała, T. Kos, P. Funk, V. Fülöpová, B. Lemrová, P. Koczurkiewicz, E. Pękala, A.J. Bojarski, P. Popik, P. Marin, P. Zajdel, Novel non-sulfonamide 5-HT6 receptor partial inverse agonist in a group of imidazo[4,5-b]pyridines with cognition enhancing properties, Eur. J. Med. Chem. 144 (2018) 716–729, https://doi.org/10.1016/j.ejmech.2017.12.053.
[31] L.I. Jiang, J. Collins, R. Davis, K.-M. Lin, D. DeCamp, T. Roach, R. Hsueh, R. A. Rebres, E.M. Ross, R. Taussig, I. Fraser, P.C. Sternweis, Use of a cAMP BRET sensor to characterize a novel regulation of cAMP by the sphingosine 1-phosphate/G13 pathway, J. Biol. Chem. 282 (2007) 10576–10584, https://doi.org/10.1074/jbc.M609695200.
[32] L. He, Q. Zhao, J. Qi, Y. Wang, W. Han, Z. Chen, Y. Cong, S. Wang, Structural insights into constitutive activity of 5-HT6 receptor, Proc. Natl. Acad. Sci. U. S. A. 120 (2023) e2209917120, https://doi.org/10.1073/pnas.2209917120.
[33] V. Isberg, C. de Graaf, A. Bortolato, V. Cherezov, V. Katritch, F.H. Marshall, S. Mordalski, J.-P. Pin, R.C. Stevens, G. Vriend, D.E. Gloriam, Generic GPCR residue numbers - aligning topology maps while minding the gaps, Trends Pharmacol. Sci. 36 (2015) 22–31, https://doi.org/10.1016/j.tips.2014.11.001.
[34] W. Pietruś, R. Kurczab, R. Kafel, E. Machalska, J. Kalinowska-Tłuścik, A. Hogendorf, M. Żylewski, M. Baranska, A.J. Bojarski, How can fluorine directly and indirectly affect the hydrogen bonding in molecular systems? – a case study for monofluoroanilines, Spectrochim. Acta Mol. Biomol. Spectrosc. 252 (2021) 119536, https://doi.org/10.1016/j.saa.2021.119536.
[35] K. Czarnota-Łydka, S. Sudoł-Tałaj, K. Kucwaj-Brysz, R. Kurczab, G. Satała, M. de Candia, F. Samarelli, C.D. Altomare, A. Carocci, A. Barbarossa, E. Żesławska, M. Głuch-Lutwin, B. Mordyl, M. Kubacka, N. Wilczyńska-Zawal, M. Jastrzębska-Więsek, A. Partyka, N. Khan, M. Więcek, W. Nitek, E. Honkisz-Orzechowska, G. Latacz, A. Wesołowska, A. Carrieri, J. Handzlik, Synthesis, computational and experimental pharmacological studies for (thio)ether-triazine 5-HT6R ligands with noticeable action on AChE/BChE and chalcogen-dependent intrinsic activity in search for new class of drugs against Alzheimer's disease, Eur. J. Med. Chem. 259 (2023) 115695, https://doi.org/10.1016/j.ejmech.2023.115695.
[36] T.T. Wager, X. Hou, P.R. Verhoest, A. Villalobos, Central nervous system multiparameter optimization desirability: application in drug discovery, ACS Chem. Neurosci. 7 (2016) 767–775, https://doi.org/10.1021/acschemneuro.6b00029.
[37] A.J. Lesiak, M. Brodsky, N. Cohenca, A.G. Croicu, J.F. Neumaier, Restoration of physiological expression of 5-HT6 receptor into the primary cilia of null mutant neurons lengthens both primary cilia and dendrites, Mol. Pharmacol. 94 (2018) 731–742, https://doi.org/10.1124/mol.117.111583.
[38] W.D. Hirst, G.W. Price, M. Rattray, G.P. Wilkin, Identification of 5-hydroxytryptamine receptors positively coupled to adenylyl cyclase in rat cultured astrocytes, Br. J. Pharmacol. 120 (1997) 509–515, https://doi.org/10.1038/sj.bjp.0700921.
[39] N.J. Allen, D.A. Lyons, Glia as architects of central nervous system formation and function, Science 362 (2018) 181–185, https://doi.org/10.1126/science.aat0473.
[40] R. Kurczab, V. Canale, G. Satała, P. Zajdel, A.J. Bojarski, Amino acid hot spots of halogen bonding: a combined theoretical and experimental case study of the 5-HT7 receptor, J. Med. Chem. 61 (2018) 8717–8733, https://doi.org/10.1021/acs.jmedchem.8b00828.
[41] Y. Cheng, W.H. Prusoff, Relationship between the inhibition constant (K1) and the concentration of inhibitor which causes 50 per cent inhibition (I50) of an enzymatic reaction, Biochem. Pharmacol. 22 (1973) 3099–3108.
[42] H.C. Cheng, The power issue: determination of *K*B or *Ki* from IC50, J. Pharmacol. Toxicol. Methods 46 (2001) 61–71, https://doi.org/10.1016/S1056-8719(02)00166-1.
[43] S. Huang, P. Xu, D.-D. Shen, I.A. Simon, C. Mao, Y. Tan, H. Zhang, K. Harpsøe, H. Li, Y. Zhang, C. You, X. Yu, Y. Jiang, Y. Zhang, D.E. Gloriam, H.E. Xu, GPCRs steer Gi and Gs selectivity via TM5-TM6 switches as revealed by structures of serotonin receptors, Mol. Cell 82 (2022) 2681–2695.e6, https://doi.org/10.1016/j.molcel.2022.05.031.
[44] wwPDB consortium, Protein Data Bank: the single global archive for 3D macromolecular structure data, Nucleic Acids Res. 47 (2019) D520–D528, https://doi.org/10.1093/nar/gky949.
[45] K.J. Bowers, E. Chow, H. Xu, R.O. Dror, M.P. Eastwood, B.A. Gregersen, J. L. Klepeis, I. Kolossvary, M.A. Moraes, F.D. Sacerdoti, J.K. Salmon, Y. Shan, D. E. Shaw, Scalable algorithms for molecular dynamics simulations on commodity clusters, in: Proceedings of the 2006 ACM/IEEE Conference on Supercomputing, Association for Computing Machinery, New York, NY, USA, 2006, pp. 84–es, https://doi.org/10.1145/1188455.1188544.
[46] M.A. Lomize, I.D. Pogozheva, H. Joo, H.I. Mosberg, A.L. Lomize, OPM database and PPM web server: resources for positioning of proteins in membranes, Nucleic Acids Res. 40 (2012) D370–D376, https://doi.org/10.1093/nar/gkr703.
[47] J.K. Singh, A. Solanki, Comparative in-vitro intrinsic clearance of imipramine in multiple species liver microsomes: human, rat, mouse and dog, J. Drug Metabol. Toxicol. 3 (2012), https://doi.org/10.4172/2157-7609.1000126.